Does Shear Induced Demixing Resemble a Thermodynamically Driven Instability?

Joseph D. Peterson, Glenn H. Fredrickson, L. Gary Leal

Department of Chemical Engineering,

University of California, Santa Barbara,

Santa Barbara, CA

Abstract: In the present paper, we continue our recent studies on a two-fluid Rolie-Poly approximation of entangled polymer solutions in simple shear flows. We review the existing literature on shear induced demixing (SID) in two-fluid models and highlight the apparent similarities to a thermodynamic model of demixing. Focusing on steady unidirectional simple shear flows driven by a constant applied shear stress, we show that when the frictional drag between solvent and polymer is asymptotically large, our two-fluid model is mathematically equivalent to a thermodynamic model in terms of its long-time concentration dynamics. In particular, we show that SID minimizes a Liapunov functional $\mathcal{L}$ distinct from the system's free energy F. We apply our asymptotic model to make predictions regarding nucleation (finite amplitude instabilities) and coalescence phenomena in SID. Numerical calculations with the full model corroborate the asymptotic model predictions. Finally, we apply the same asymptotic analysis to two flows in which a thermodynamic mapping fails. First, we consider steady simple shear flows driven by a constant boundary velocity (as opposed to a constant boundary stress), wherein the hydrodynamic instability appears to have the same character but can no longer be mapped to an equivalent thermodynamic instability. Second, we consider unsteady simple shear flows driven by an oscillating boundary stress, wherein the non-linear dynamics of demixing are totally distinct from what a thermodynamic model predicts.

1. Introduction

When a thermodynamically stable mixture of polymer and solvent is subjected to simple shear flow, there are circumstances under which the material may become hazy/turbid, indicative of compositional inhomogeneity present over long length scales. In some respects, the induced turbidity resembles what emerges in a quiescent system approaching the cloud point of a phase transition. Indeed, early explorations of this phenomena [1] considered the optical turbidity to be a universal signature of an incipient phase transition, and explained its emergence in flow via a relatively simple line of reasoning: (1) phase transitions occur to minimize the free energy of a system, (2) polymers in flow have an elastic free energy not present at equilibrium, therefore (3) the phase diagram for a polymeric system in flow must be shifted relative to its equilibrium position. The subtle problem with this reasoning is that (1) is not generally true for externally forced systems (e.g. systems under flow). Thus, while it is true that flow will change the free energy of the system in some way, the free energy cannot necessarily be used to predict phase transitions for systems under flow.

As the weaknesses of such quasi-thermodynamic ideas became apparent, attention turned toward more general 'two-fluid' models of polymer solutions [2] [3] [4] [5] [6]. In a two-fluid model, polymer migration arises naturally via competition between the elastic, osmotic, and drag forces acting on the polymers. Through this new framework, it was discovered (and confirmed experimentally) that flow-induced turbidity can occur by stress-enhanced concentration fluctuations (SECF), with no need for an induced phase transition. It is worth noting, however,

that SECF does not explain all experimentally observed instances of flow-induced inhomogeneity – some systems do seem to show that shear can induce the formation of a second phase that persists for long times after the cessation of flow (see [1] and references therein).

More recent studies of two-fluid models in flow have shown that, under certain conditions, one can predict the existence of a linear shear-induced demixing (SID) instability, where demixing is in fact suggestive of a flow-induced shift in the equilibrium phase diagram [7] [8] [9] [10] [11] [12] [13] [14] [15]. These demixing instabilities are distinct from SECF in that the system develops a 'banded' concentration profile that ages with time, and continuous fluctuations are not required to maintain compositional inhomogeneity at steady state. For these SID instabilities, an apparent similarity to quiescent phase transitions does not imply that SID is thermodynamically driven in any sense, but thermodynamic intuitions of phase transitions seem to describe most of the observed dynamics (at least for the case of steady simple shear flow). Clear experimental evidence of SID can be found in the work of Migler, Liu, and Pine [16].

Overall, it seems that SID has a paradoxical nature of sorts – while the instability is not thermodynamic in nature, for all practical purposes it seems to behave as though it were. In the present report we consider this paradox and produce some new understanding; we show that for a certain asymptotic limit of our two-fluid model, one can compute a Lyapunov functional (distinct from the free energy) that is minimized during SID for steady simple shear flows driven by a constant shear stress. This allows for an exact mapping between SID and the analogous problem of demixing in quiescent systems. We then show that the resulting asymptotic model of SID is in agreement with the full model predictions; the agreement is quantitative with respect to stability boundaries and steady states, and qualitative with respect to the intermediate dynamics.

Thus, the dynamics of the instability are mathematically similar to a thermodynamically driven instability, in spite of the fact that the instability is not thermodynamic in nature.

A key point is that the asymptotic model of SID creates a useful link to results that are well established for thermodynamically driven instabilities but are still open questions for SID. Two of the most important outstanding questions for SID instabilities are the local stability of inhomogeneous states (related to coarsening) and the local and global stability of homogeneous states (related to nucleation and spinodal decomposition) for macroscopic systems. These can be challenging problems to probe in a nonequilibrium system, but are essential for understanding how SID is likely to manifest in experimental contexts.

On the first point, we shall see that the asymptotic model predicts that demixing instabilities always lead to bulk phase separation, as any system containing many small bands is always linearly unstable to further coarsening. On the second point, the asymptotic model predicts that the stability boundary for SID may not be sharply resolved in experiments: finite amplitude fluctuations can tip a locally stable system towards demixing when it is sufficiently 'close' to a linear stability boundary. For SID in steady simple shear flow, numerical simulations of the full model are consistent with these predictions.

In spite of the apparent success of thermodynamic intuitions for SID in simple shear flows, it is critical that one remain cautious when extrapolating to systems for which the validity of such intuitions has yet to be established. To this point, the present manuscript offers two examples for further consideration.

As a first example, the above-mentioned results hold true for steady simple shear flows driven by a constant shear stress, but it is as-yet unknown whether the global stability results still hold true for shear flows driven by a constant wall velocity. When exchanging constraints related to external forcing, a Legendre transformation does not yield a new potential to be minimized (as it does for equilibrium systems). The complication is that shear stress and wall velocity are not conjugate variables for inhomogeneous shear flows (i.e. he overall shear rate bears no relation to how an 'effective' free energy responds to changes in the stress). As a result, Legendre transforms cannot serve the same purpose for which they are often employed in equilibrium systems. Therefore, in spite of the fact that simulations of SID show qualitatively similar results for the two modes of deformation, it may be that SID is not mathematically congruent to a thermodynamic phase separation under conditions of fixed overall shear rate.

As a second example, we show that steady simple shear flow appears to be a special case in the sense that an asymptotic model is not necessarily predictive far from the relevant asymptotic limit in other flow types. For a particularly telling example, we employ the same methods of analysis to construct an asymptotic model of SID instabilities in large amplitude oscillatory shear flows (LAOS) driven by an oscillating boundary stress. For this final case, we find that the resulting asymptotic model is useful for predicting and explaining the onset of SID instabilities, but generally inadequate for describing the dynamics that follow.

2. Background

2.1. The two-fluid model approximation and stress-induced migration

Two-fluid models are a phenomenological but historically successful means of describing compositionally inhomogeneous complex fluids [17] [2] [6] [4]. For the present study, we focus on a two-fluid model of semi-dilute entangled polymer solutions (very long chains that are well entangled but present in low volume fractions) as considered in our previous work [9] [10] [18] [13]. In a two-fluid model, the molecular details of each species (polymer and solvent) are coarse-grained into a continuum model, in which all species are treated as co-continuous, interpenetrating continuum fluids, coupled together by drag forces and by an incompressibility constraint. In this framework, predictions of polymer migration arise naturally via a force balance on the polymer fluid component.

The phenomenological two-fluid approximation is reasonably justified for the case of semi-dilute entangled polymer solutions: the polymers do experience drag forces with the solvent, the overall solution is nearly incompressible, and the mesh-like structure of the entangled polymers makes the two components effectively co-continuous. In several notable cases, the predictions of two-fluid models have been successfully validated against experiments on semi-dilute polymer solutions [2] [4] [19] [20] [16].

2.2. Shear induced demixing in two-fluid models: Linear stability predictions

Simple shear flow is often considered to be free of stress gradients, and so it is not immediately obvious how stress induced migration would be occur in such a flow. While it is true that there are no macroscopic stress gradients from the geometry itself, stress gradients can

still arise on microscopic length-scales through amplification of the effects of thermal fluctuations in the system. For example, if the polymer concentration is slightly perturbed from homogeneity by a thermal fluctuation, the velocity field will become slightly perturbed as well (assuming a composition-dependent viscosity). This, in turn, perturbs the elastic stresses in the system and creates the opportunity for stress-induced migration up concentration gradients [2]. This mechanism for stress induced migration in simple shear flows describes both SECF (where all linear perturbations eventually decay) and SID (where some perturbations are linearly unstable). Here, we are exclusively interested in the latter case.

SID instabilities in two-fluid models have been studied for a range of different entangled polymeric materials, including wormlike micelles [7] [8], polymer blends [11] [12] [21], and polymer solutions [9] [10] [13], and it is fair to say that this aspect of the phenomenon is well understood. Although there are some subtle differences with regard to the underlying equations and the resulting predictions, the most important qualitative predictions appear to be transferrable among the three cases. For these materials, a linear instability to demixing first develops at shear rates around the inverse reptation time, when normal stresses are large and shear thinning is present. Under such conditions, the system exhibits a rheological "plateau", and small changes in concentration can lead to relatively large changes in shear rate, with regions of low/high concentration having higher/lower shear rates. This leads to the polymer being more deformed in regions of low concentration, and less deformed in regions of high concentration. As a result, the polymer's normal stresses are larger in regions of lower concentration, which promotes migration up concentration gradients, and a demixing instability is inevitable if osmotic stresses are sufficiently weak (i.e. when the solvent quality is sufficiently poor) [13].

When a linear instability to demixing occurs, inhomogeneous domains develop with a preferred wavelength (fastest growing linear mode), and unstable modes are always oriented in the flow gradient direction [4]. The preferred wavelength in the linear regime is ultimately set by a balance of capillary limitations (suppressing short wavelength modes) and diffusive limitations (suppressing long wavelength modes). In purely diffusive systems, the lengthscale for capillary effects (i.e. the solution correlation length ξ) sets the preferred wavelength for demixing, but for viscoelastic systems the preferred wavelength is often substantially longer.

To understand how a preferred wavelength is selected in an entangled viscoelastic system, it is worthwhile to consider the effects of 'migration induced stress': demixing arises via dilations of the mesh, and these dilations are rightly viewed as a secondary deformation (hence the term 'migration induced stress') that feeds back into the absolute elastic stress and attenuates further migration. In the context of selecting a preferred wavelength for demixing, the stress incurred by migration must be allowed to relax before additional migration can take place. Stress relaxation is generally growth limiting for perturbation wavelengths larger than the solution correlation length ξ (where capillary forces limit growth) but smaller than the 'magic length' ℓ_C (where diffusion is growth limiting). The 'magic length' ℓ_C is simply the length-scale at which diffusion and stress relaxation happen at the same time-scale [20], and can be defined relative to the equilibrium diffusion coefficient D_{eq} and terminal relaxation time τ_D as $\ell_C^2 = D_{eq}\tau_D$.

When the magic length is much longer than the solution correlation length, $\ell_C/\xi \gg 1$, the preferred wavelength for demixing tends to scale as the geometric mean of the two, $[\ell_C\xi]^{1/2}$. The effects of migration induced stress on wavelength selection have been previously documented in demixing of viscoelastic mixtures, irrespective of whether demixing is driven by

hydrodynamic or thermodynamic forces [8] [22] . Overall, the initial linear instability to SID in two-fluid models is well understood at this time, but important aspects of the non-linear dynamics require further attention.

2.3. Shear induced demixing in two-fluid models: Non-linear predictions

Although linear stability analysis is useful for determining the length scale and orientation at which inhomogeneity first develops, at longer times the perturbation will grow to the point where non-linear effects are important, and analysis of the linear instability is no longer predictive. At this point, there are few (if any) established analytical results for the non-linear dynamics of SID in two-fluid models, and most of what is known has been established via numerical simulations.

Indeed, in spite of the significant effort to simulate the nonlinear evolution of SID, the present understanding of SID is still incomplete. What is lacking (and what will be the focus of this paper) is an understanding of non-linear stability in homogeneous states (nucleation and growth mechanisms for demixing) and linear stability of inhomogeneous states (long time coarsening dynamics in macroscopic systems). In the paragraphs that follow, we discuss the experimental relevance of these questions as well as the difficulty of addressing them through numerical simulations alone.

First, when quasi-statically increasing the applied shear rate from zero, when does one first encounter a demixed flow, and how does it form? Will the system only demix when the linear stability boundary is encountered, or will a finite amplitude instability cause demixing to occur prior to that point? For thermodynamically-driven demixing instabilities, it is well known that

macroscopic phase separation always reduces the system's free energy, and homogeneous systems that are locally stable but capable of being demixed will inevitably demix by finite amplitude instabilities (nucleation) if given a sufficiently long waiting time. In equilibrium systems, comparing the relative stability of locally stable systems is easy – one only needs to compare the free energy of the two states. In non-equilibrium systems, however, this is generally a much harder problem. However, if thermodynamic intuitions of SID are valid, then it should be possible to use the mathematical tools of equilibrium thermodynamics to assess the relative stability of all available steady states.

Second, after the onset of an SID instability, the perturbation grows until the flow is comprised of distinct 'bands' of high/low polymer concentration, oriented in the flow gradient direction. Transitions between high/low concentration bands develop over a small interfacial length-scale (the solution correlation length ξ for our model). After the bands form, simulations show that there is a tendency (at least initially) for the bands to ripen together, decreasing the total number of bands and increasing the average size of a band. Some simulations have suggested that the ripening process terminates before bands become macroscopic, but these simulations were of relatively short duration [11] [12] or contained thermodynamically inconsistent interfacial stresses [10]. The open question is whether the system will ripen towards a macroscopically banded state, or is there a preferred intermediate size for which the shear bands are most stable? As we have already mentioned, existing simulations show a clear tendency for bands to ripen initially but the long-time behavior is still an open problem, in our opinion. Furthermore, it is unlikely that this question could be resolved with numerical simulations alone; coarsening becomes prohibitively stiff (temporally and spatially) when the

gap dimension is exceedingly large relative to the typical interfacial width. However, if thermodynamic intuitions of SID are valid, then scaling laws for coarsening dynamics are well-established [23] [24].

2.4. Dynamics of Demixing in a Fluid Mixture at Rest

To the reader familiar with thermodynamically driven demixing instabilities [15] [23] [25], much of what we have described for SID may evoke strong parallels to the linear and non-linear dynamics of thermodynamically-driven demixing instabilities. With regards to the linear instability, both systems demix with a preferred wavelength that is set by a balance of diffusive effects (favoring short wavelengths) and capillary effects (favoring long wavelengths). With regards to nonlinear dynamics, both systems show a tendency to coarsen towards a state involving two locally homogeneous regions.

To the reader unfamiliar with the dynamics of thermodynamically driven phase transitions, we have provided an appendix to review a number of important 'textbook' results. Specifically, we review predictions for model B of the Halperin-Honenberg classification scheme [25]. In the appendix, we confirm that the free energy F is minimized by the dynamics of model B, we derive the conditions for linear instability, and we show how a 'common tangent' construction can be used to obtain the compositions of phases in equilibrium.

If an analogy between SID and model B phase transitions can be rigorously supported, then the two important questions on SID, discussed above, can be trivially answered. For model B systems, demixing is the most favorable state of the system whenever a phase separated solution exists – if the same is true for SID, then (given a sufficiently long waiting time for a system with

'noise') a high shear band will first nucleate at the lowest possible shear rate for which inhomogeneous steady states exist. Second, for model B systems, any demixed state that is incompletely coarsened is linearly unstable – if the same is true for SID, then SID will eventually produce macroscopic shear banding if given sufficient time.

3. Flow-Induced Concentration Inhomogeneity in a Semi-Dilute Polymer Solution for 1D Shear Flows with a Constant Wall Shear Stress

3.1. Governing Equations for the 2-Fluid Model

The full tensorial governing equations for our two-fluid model of a semi-dilute entangled polymer solution (good solvent conditions) have been derived in a series of previous papers from our group [13]. The derivation largely follows the 'Rayleighan' method as outlined by Doi and Onuki [5]. In keeping with our previous work, we will employ the so-called '1D' approximation in which spatial variations of composition, velocity, etc. are assumed to occur only in the flow gradient direction. This '1D' approximation greatly simplifies the problem, and is adequate to describe both the conditions for linear instability and the 'banded' structure observed at long times after demixing.

Here, we present the equations for study of '1D' simple shear flows, where the homogeneous state is a unidirectional shear flow, $\boldsymbol{u}(x,y,z) = u(y,t)\boldsymbol{i_x}$, with a uniform polymer volume fraction, ϕ_o. The flow is assumed to be inertialess, i.e. the Reynolds number is vanishingly small. Relative to other two-fluid models of polymeric systems, our model primarily differs in its choice of constitutive model (Rolie Poly), which is a modern standard for single-mode, tube-

based models of entangled polymer rheology [26] [27]. The Rolie Poly model is best suited to describe well-entangled and monodisperse linear chain polymer melts and solutions (e.g. more than ten tube segments per chain). For polymers that are unentangled, weakly entangled, polydisperse and/or branched, a different two fluid model should be employed.

The governing equations presented here have been nondimensionalized following an appropriate selection of characteristic scales as outlined in our prior work [13]. The relevant dimensionless groups governing the problem are the Weissenberg number Wi (strain rate relative to reptation-based stress relaxation rate), viscosity ratio ϖ (solvent viscosity relative to polymer viscosity), relaxation time ratio θ (reptation time relative to Rouse reorientation time, approximately equal to $3Z$, where Z is the average number of 'tube' segments per chain), and moduli ratio E (elastic modulus relative to osmotic modulus). There are also two metrics of the system size, comparing the gap dimension to relevant microscopic length-scales: $\overline{H}/\bar{\xi}$ (gap dimension H relative to solution correlation length ξ), and $\overline{H}$ (gap dimension H relative to the 'magic length', ℓ_C). A full table of all variables used in the present report can be found in the appendix.

For reference, the full governing equations are listed below, and variables are defined as follows:

$t =$ time (normalized by $\tau_D(\phi_o)$, the reptation time of a polymer solution at its mean polymer volume fraction ϕ_o)

$y =$ gap position (normalized by H, the system size)

$\phi =$ polymer volume fraction (normalized by ϕ_o)

u_P = polymer velocity in the flow direction (normalized by $H/\tau_D(\phi_o)$ so that the dimensionless velocity at the moving wall is equal to the Weissenberg number, Wi)

u_S = solvent velocity in the flow direction (normalized by $H/\tau_D(\phi_o)$)

v_P = polymer velocity in the flow gradient direction (normalized by $\phi_o^2\chi_o^{-1}/\zeta(\phi_o)H$, where χ_o^{-1} is the osmotic susceptibility and $\zeta(\phi_o)$ is the drag coefficient for polymer and solvent for a polymer solution with polymer volume fraction ϕ_o)

Q_{ij} = the ij component of the polymer conformation tensor.

Π_{ij} = the ij component of the total polymer stress tensor (including both elastic and osmotic effects).

$$\frac{\partial\phi}{\partial t} = -\frac{1}{\bar{H}^2}\frac{\partial}{\partial y}(\phi v_P) \qquad (1)$$

$$0 = \frac{\partial}{\partial y}\left[\Pi_{xy} + E\varpi\frac{\partial u_S}{\partial y}\right] \qquad (2)$$

$$u_P - u_S = \frac{1}{\bar{H}^2}\left[\phi^{-\frac{3}{2}}\frac{\partial\Pi_{xy}}{\partial y}\right] \qquad (3)$$

$$v_P = \phi^{-3/2}\frac{\partial\Pi_{yy}}{\partial y} \qquad (4)$$

$$\Pi_{xy} = E\phi^{9/4}Q_{xy} \qquad (5)$$

$$\Pi_{yy} = E\phi^{9/4}\left[\left(Q_{yy}-1\right) + \frac{5}{8}(\mathrm{tr}(\boldsymbol{Q}) - 3 - \ln(\det(\boldsymbol{Q})))\right] - \frac{1}{2}\phi^2 + \left(\frac{\bar{\xi}}{\bar{H}}\right)^2\phi^{-\frac{3}{2}}\left[\phi\frac{\partial^2\phi}{\partial y^2} - \frac{5}{4}\left|\frac{\partial\phi}{\partial y}\right|^2\right] \qquad (6)$$

$$\frac{\partial Q_{xx}}{\partial t} + \frac{1}{\bar{H}^2} v_P \frac{\partial Q_{yy}}{\partial y} - 2Q_{xy}\frac{\partial u_P}{\partial y} = -R_{xx} \qquad (7)$$

$$\frac{\partial Q_{yy}}{\partial t} + \frac{1}{\bar{H}^2}\left[v_P \frac{\partial Q_{yy}}{\partial y} - 2Q_{yy}\frac{\partial v_P}{\partial y}\right] = -R_{yy} \qquad (8)$$

$$\frac{\partial Q_{zz}}{\partial t} + \frac{1}{\bar{H}^2} v_P \frac{\partial Q_{zz}}{\partial y} = -R_{zz} \qquad (9)$$

$$\frac{\partial Q_{xy}}{\partial t} + \frac{1}{\bar{H}^2}\left[v_P \frac{\partial Q_{yy}}{\partial y} - Q_{xy}\frac{\partial v_P}{\partial y}\right] - Q_{yy}\frac{\partial u_P}{\partial y} = -R_{xy} \qquad (10)$$

$$R_{ij} = \phi^{-3/2}\left(Q_{ij} - \delta_{ij}\right) + 2\theta\left(1 - \frac{1}{\lambda}\right)\left(Q_{ij} + \frac{1}{\lambda}\left(Q_{ij} - \delta_{ij}\right)\right) \qquad \lambda = \left[\frac{1}{3}\mathrm{tr}(\boldsymbol{Q})\right]^{1/2} \qquad (11)$$

To represent an imposed flow, we are primarily interested in simple start-up protocols, where a system begins at rest and is then deformed with a constant wall velocity or a constant applied shear stress. In both cases, we set $u_S(y=0) = 0$, and for the former case, we use $Q_{xy} + \varpi \partial u_S/\partial y = \Sigma_0$ at $y = 1$ while the latter case uses $u_S(y=1) = 1$.

For the purposes of the present report, we solve equations (1) - (11) using Lees Edwards boundary conditions [28], which are an analogue to periodic boundary conditions for systems in simple shear flow. All variables except u_P and u_S are assumed to be periodic, while u_P and u_S have a 'jump' discontinuity across the boundary [28], since the imposed deformation requires a net increase in the flow velocity from $y = 0$ to $y = 1$. More details on the choice of boundary conditions is given in an appendix for the interested reader.

Finally, the polymer concentration and conformation also require initial conditions; in general, we choose to have the polymer conformation initialized at its equilibrium state while a

small amount of random noise is introduced into an otherwise uniform initial concentration profile.

From a cursory inspection, it is not immediately obvious that the governing equations of our two-fluid model should be reducible to any thermodynamically driven model of demixing (as numerical results seem to show). For comparision, model B of the Halperin-Honenberg classification scheme [25] is a simple model for thermodynamically driven demixing instabilities. For model B, transport occurs via migration down chemical potential gradients, and in 1D the polymer volume fraction would evolve as:

$$\frac{\partial}{\partial t}\phi = \frac{\partial}{\partial y}\left[M(\phi)\frac{\partial}{\partial y}\left[\frac{\delta F}{\delta \phi}\right]\right] \qquad (12)$$

where $M > 0$ is the species mobility, F is the system free energy, and t, y are temporal and spatial coordinates. In the present paper we seek to illuminate an underlying relationship between SID in the full two-fluid model (eqn. (1) - (11)) and thermodynamically driven demixing as described by model B (eqn. (12)).

Having presented our version of a two-fluid model, the interested reader may wonder how the conclusions of our paper can be generalized to other two-fluid systems. In our view, the analysis that we perform here should be transferrable to any viscoelastic multi-fluid model free of constitutive instabilities (i.e. homogeneous shear banding) [4] [7] [11] [29] [21] [30] [31]. There may be significant quantitative differences with regard to the conditions under which SID instabilities occur, but the main qualitative conclusions (regarding whether SID resembles a thermodynamically driven instability) should not be sensitive to one's choice of two-fluid model.

3.2. The Analogy Between SID and Model B

If there are mathematical similarities between model B phase separations and SID in our two-fluid model, it is worthwhile to revisit insights of Rangel-Nafaile et al. and present a more rigorous framing for their quasi-thermodynamic hypothesis of SID [1]. Their hypothesis, roughly summarized, was that the system evolves to minimize its total free energy, even in the presence of dissipative external forcing (flow). In the absence of any non-equilibrium dynamical equations (such as those in the preceding section), this hypothesis may be a useful starting point, but it has no actual basis in non-equilibrium thermodynamics or statistical mechanics. However, given a set of dynamical equations for any arbitrary system, it is sometimes possible to find a 'Lyapunov functional' to those equations. In such cases, the Lyapunov functional can be used as a non-equilibrium surrogate for thermodynamic intuitions of energy minimization [32] (e.g. the state with the lowest value of the Lyapunov functional will always be the most stable)

For a given set of dynamical equations, a Lyapunov functional $\mathcal{L}$ has the property of being strictly non-increasing along any deterministic trajectory of the system, $\partial\mathcal{L}/\partial t \leq 0$. In this sense, one can say that the dynamics of the system evolve to minimize $\mathcal{L}$. Stationary solutions to the dynamics are found at local minimums of $\mathcal{L}$, and the global stability of these stationary solutions can be ranked in order of decreasing $\mathcal{L}$. For a quiescent system (no external forcing), the laws of thermodynamics require that $\partial F/\partial t \leq 0$ and so it is trivial to show that the free energy of such a system is a Lyapunov functional for its dynamics. In this case, the criterion for local and global stability distinguish true equilibrium states from thermodynamically unstable

and metastable states. By analogy, we can refer to a Lyapunov functional as an 'effective' free energy for systems subject to external forcing.

With this in mind, we can reframe the hypothesis of Rangel-Nafaile et. al. [1] in a way that requires no heuristic assumptions of non-equilibrium thermodynamics. Formally, we hypothesize that the equations of motion for inhomogeneous polymer solutions in shear flow possess a Lyapunov functional $\mathcal{L}$ that differs from the equilibrium Lyapunov functional F by an additive, local (bulk) contribution, $\Lambda(\phi, \Sigma)$, that depends only on the local composition and the instantaneous flow protocol:

$$\mathcal{L} = \int_0^H dy \, (f_L(\phi) + \Lambda(\phi, \Sigma) + f_{NL}(\phi, \nabla\phi)) \qquad (13)$$

where Σ is the flow protocol defined in terms of an applied wall stress in this case. The function Λ would represent a flow-induced shift to an *effective* free energy landscape governing the dynamics of mixing/demixing within the system. Note, however, that $\mathcal{L}$ is not the *actual* free energy of the system. This is the key distinction between the analysis presented here and the original work of Rangel-Nafaile et al. If such a form of $\mathcal{L}$ exists for steady simple shear flow, then for the 1D case there would be no mathematically discernible difference between SID and a model B phase transition. For the remainder of this paper, the equivalence of SID and model B in 1D is referred to as the quasi-thermodynamic hypothesis of shear induced demixing (QTH).

Framed in this way, it is easy to point out that QTH fails even for the kinetics of demixing during the first stages of spinodal decomposition. When selecting a preferred wavelength for demixing, the effects from migration-induced stress (selectively attenuating the growth of short wavelength modes) cannot be reduced to a shift in the effective free energy of mixing, since the

free energy penalty for such perturbations is assumed to be independent of the perturbation wavelength. Therefore, we suggest that a better understanding of shear induced demixing may be found in a weaker version of QTH (wQTH) that still preserves the original thermodynamic intuition. In two parts, we propose wQTH as follows:

(a) QTH is true for some asymptotically limiting cases of SID

(b) Away from the relevant asymptotic limit in (a), the correspondence between SID and model B is not exact, but any distinctions are strictly quantitative, and the essential qualitative physics of the underlying transition and its dynamics are unchanged.

In the work that follows, we will show that there are some flow protocols for which wQTH appears to hold true, some where it does not, and others where it is uncertain. Each of these cases are interesting and important in their own right; when wQTH appears to be true (as we will show for simple shear flow with constant shear stress), it allows us to answer questions about global stability analysis and asymptotic coarsening dynamics, as previously discussed. When wQTH is demonstrably false (as we will show for LAOS flows), it opens up opportunities for experimental validation of non-trivial predictions from the numerical simulations. And finally, for the case of fixed wall velocity (as opposed to fixed stress) wQTH is uncertain because the well-developed tools for exchanging constraints in thermodynamic systems (Legendre transforms) do not apply for exchanging constant shear stress for constant shear rate.

In the work that follows, we will prove QTH in simple shear flow for a two-fluid model in the limit of high coupling friction ($\bar{\xi} \gg 1$ for fixed $\bar{H}/\bar{\xi}$). We will then compare simulations of the asymptotic model with the full model for both large and small (realistic) coupling frictions, with some discussion for why QTH appears to hold when the coupling friction is not large

(hence demonstrating wQTH). This work allows for a concise resolution to several outstanding problems in 1D SID, to which we have previously alluded. A representative set of simulation results are also provided to support the conclusions of this analysis. Finally, the methods used for proving wQTH in simple shear flow are applied to oscillatory shear flows, and supporting simulation results are given.

3.3. The Limit of Large Coupling Friction: Proof of QTH for this Case in 1D Steady Shear Flows

It has long been recognized that much of the essential behavior of a two-fluid model is preserved under the so-called 'adiabatic approximation' [2] [4] [14]. Under this approximation, the fluid's viscoelastic constitutive behavior is replaced with a purely rate-dependent constitutive law having the same steady state response. This approximation provides a sensible strategy for slaving changes in stress to changes in composition, which greatly simplifies the governing equations. Here, we show that for 1D steady simple shear flow, the adiabatic approximation can be formally constructed by considering the asymptotic limit of large coupling friction between the polymer and solvent.

In our 1D two-fluid model, the coupling friction controls the rate of diffusion but not the rate of stress relaxation. When the coupling friction is made to be very large, the characteristic time-scale for mass transport can be asymptotically separated from the characteristic timescale for stress relaxation. On time-scales relevant to stress relaxation, mass transport effects can be neglected – the coupling friction is so large that the polymer concentration appears to be 'frozen' in time. At longer time-scales, mass transport effects are evident, but viscoelastic transients are not – the velocity profile and polymer conformation respond quasi-statically to changes in

polymer concentration. Therefore, when the system is viewed on time-scales relevant to mass transport, the asymptotic limit of large coupling friction is functionally equivalent to the classical adiabatic approximation.

In our dimensionless two-fluid model, the coupling friction is encoded in the magic length that appears in $\bar{\xi}$ and $\bar{H}$. When the coupling friction is asymptotically large, the magic length becomes asymptotically small, since polymers are unable to migrate any significant distance on the time-scale of stress relaxation. Thus, in the high coupling friction limit, both $\bar{\xi}$ and $\bar{H}$ become asymptotically large while their ratio remains fixed (i.e. $\bar{\xi} \gg 1$ for fixed $\bar{H}/\bar{\xi}$).

In a physically realistic description of semi-dilute polymer solutions, the coupling friction cannot be increased independently from the stress relaxation time, since the two are mutually dependent on the solvent viscosity. If the polymer has a mesh size of ξ and the solvent has a viscosity μ_S, then the overall drag coefficient between the polymer and the mesh must be given by $\zeta \sim \mu_S/\xi^2$ [17]. Furthermore, by definition, the drag coefficient ζ must be related to the magic length by:

$$D_{eq} = \frac{\phi_o^2 \chi_0^{-1}}{\zeta} = \frac{\ell_C^2}{\tau_D}$$

where D_{eq} is the equilibrium coefficient of diffusion. Rearranging, we find:

$$\phi_o^2 \chi_0^{-1} \frac{\xi^2}{\mu_S} = \frac{\ell_C^2}{\tau_D}$$

$$\frac{\xi^2}{\ell_C^2} = \frac{\mu_S}{\phi_o^2 \chi_0^{-1} \tau_D} = \left(\frac{\mu_S}{G(\phi_o)\tau_D}\right)\left(\frac{G(\phi_o)}{\phi_o^2 \chi_0^{-1}}\right) = \varpi E$$

Thus, the quantity $\bar{\xi} = \xi/\ell_C$ should be constrained by $\bar{\xi} \sim [E\varpi]^{1/2}$. Since semi-dilute entangled polymer solutions typically have $\varpi \ll 1$, the asymptotic limit of high coupling friction ($\bar{\xi} \gg 1$ for fixed $\bar{\xi}/\bar{H}$) is the opposite of the physically relevant asymptotic limit ($\bar{\xi} \ll 1$). Nonetheless, we will show that the asymptotic model exactly captures stability boundaries in the macroscopic limit ($\bar{H} \gg 1$) and is quantitatively useful for predicting steady state banded concentration profiles to $\mathcal{O}(\varpi)$. For the intermediate dynamics, changing the coupling friction quantitatively effects the course of demixing (e.g. changing the timescales and lengthscales that one observes) but does not generally change the available homogeneous/inhomogeneous steady states or their linear stability. Therefore, the qualitative progressions of demixing and coarsening are left intact, in spite of any potentially unrealistic choice of coupling friction.

To resolve composition changes in the limit of high coupling friction, we re-scale the temporal axis to obtain a dimensionless diffusive timescale $\tau = t/\bar{H}^2$. After rescaling, the momentum balance equations are unchanged, but the re-scaled transport equation (1) is now given by:

$$\frac{\partial \phi}{\partial \tau} = -\frac{\partial}{\partial y}(\phi v_P) \qquad (14)$$

and the constitutive equations by:

$$\frac{1}{\bar{H}^2}\frac{\partial Q_{ij}}{\partial \tau} + \cdots = -R_{ij}. \qquad (15)$$

For fixed $\bar{\xi}/\bar{H}$, we can define a small parameter in the limit of asymptotically large coupling friction as $\epsilon = 1/\bar{H}^2$. We then seek an asymptotic solution to the governing equations in the

limit of $\epsilon \ll 1$. For the polymer volume fraction (and other independent variables), we define the asymptotic series:

$$\phi(\tau, y, \epsilon) = F_0(\epsilon)\phi_0(\tau, y) + F_1(\epsilon)\phi_1(\tau, y) + F_2(\epsilon)\phi_2(\tau, y) + \cdots \qquad (16)$$

Here ϕ_0 is the leading order solution (with gauge function $F_0(\epsilon)$), ϕ_1 is the first correction (with gauge function $F_1(\epsilon)$) and so on. Asymptotic series for other variables are defined with the same subscript notation. Because the polymer volume fraction is non-vanishing in the limit of $\epsilon \to 0$, we know that $F_0(\epsilon) = 1$, and the $\mathcal{O}(1)$ equations are given by:

$$\frac{\partial \phi_0}{\partial \tau} = -\frac{\partial}{\partial y}\left(\phi_0 v_{P,0}\right) \qquad (17)$$

$$\Sigma_0 = \Pi_{xy,0} + E\varpi \frac{\partial u_{S,0}}{\partial y} \qquad (18)$$

$$u_{P,0} = u_{S,0} \qquad (19)$$

$$v_{P,0} = \phi_0^{-3/2} \frac{\partial \Pi_{yy,0}}{\partial y} \qquad (20)$$

$$2Q_{xy,0} \frac{\partial u_{P,0}}{\partial y} = R_{xx,0} \qquad (21)$$

$$0 = R_{yy,0} = R_{zz,0} \qquad (22)$$

$$Q_{yy,0} \frac{\partial u_{P,0}}{\partial y} = R_{xy,0} \qquad (23)$$

The tensor components $\Pi_{ij,0}$ and $R_{ij,0}$ are defined as before, but now in terms of ϕ_0 and $Q_{ij,0}$ instead of ϕ and Q_{ij}. For boundary conditions, we choose Lees-Edwards and constant shear stress, Σ_0, as described by equations **Error! Reference source not found.** - **Error! Reference**

source not found.. We also solve the total momentum balance equation (18) in its integrated form at each point.

One may note that highest order time derivatives have been lost in the governing equation for the conformation tensor. This means that at $\tau = 0$ we can no longer impose an initial condition; instead, there must be some temporal boundary layer within which the initial conditions can be applied and viscoelastic start-up transients can be resolved. We therefore recognize the approximate solution in terms of $\epsilon \ll 1$ as a singular asymptotic expansion. In the language of such solutions, the expansion (16) is relevant to the "outer" - i.e. long-time - approximation. The equations (1) - (11) in terms of time t (scaled with the reptation time) are the basis of the "inner" asymptotic solution. Without knowledge of the 'inner solution' and a proof of matching with the 'outer solution', it is not a priori obvious that the governing equations presented above can be considered a valid asymptotic description of the high coupling friction dynamics of the full model. In the interest of concise exposition, we do not show the full details of the short-time startup problem here, but we ask the interested reader to consult the appendices where this analysis is given in detail, including the matching condition with the inner solution,

$$(\text{inner solution})_{t\gg 1} \Leftrightarrow (\text{outer solution})_{\tau\ll 1} \quad \text{in the limit } \epsilon \to 0 \qquad (24)$$

In broad strokes, the matching process goes as follows: The inner solution resolves viscoelastic transients but excludes polymer migration to leading order. At long times, the inner solution approaches a steady state solution for the fixed (potentially inhomogeneous) concentration profile. If this same concentration profile is used as the initial condition to the outer solution, then at $\tau = 0$ the conformation tensor and velocity profile exactly match with the steady state solution of the inner problem. For $\tau > 0$, as long as the initial perturbation is

smooth, the dynamics of the outer solution are also smooth about $\tau = 0$. When the dynamics are smooth, they can be Taylor expanded, and so the mismatch is found to be $\mathcal{O}(\epsilon)$ for $\tau \ll 1$. This mismatch determines the gauge function for the first correction to the inner solution, and further corrections to the inner/outer solutions can be obtained.

Returning to the governing equations in the limit of high coupling friction (the outer equations, (17)- (23)), we see from (19) that the polymer and solvent have the same velocity in the direction of the undisturbed/base flow. Considering the total momentum balance equation (18) and the constitutive equation (21) - (23), we also see that the polymer conformation tensor is always at steady state with respect to the local composition and applied shear stress:

$$Q_{ij,0}(\tau, y) = Q_{ij}^{SS}(\phi_0(\tau, y), \Sigma_0) \qquad (25)$$

The same is also true of the total polymer stress tensor:

$$\Pi_{ij,0}(\tau, y) = \Pi_{ij}^{SS}(\phi_0(\tau, y), \Sigma_0) \qquad (26)$$

This is equivalent to the usual adiabatic approximation. We also point out that the preceding steps have assumed a monotonic (invertible) relationship between the steady state shear stress and shear rate. A more careful analysis of the $\epsilon \ll 1$ limit is required for fluids with homogeneous shear banding instabilities.

At this point, the concentration equation can be written as:

$$\frac{\partial \phi_0}{\partial \tau} = -\frac{\partial}{\partial y}\left[\phi_0^{-1/2}\frac{\partial}{\partial y}\Pi_{yy}^{SS}(\phi_0, \Sigma_0)\right] \qquad (27)$$

With periodic boundary conditions, the above is a well-posed PDE for the polymer volume fraction in solution. By inspection, we may anticipate some similarities to the structure of model

B, as defined in equation (12). It is perhaps intuitively obvious that there should be very similar physics to model B in this limit where the viscoelastic stress (and flow) only evolve in response to the slowly developing concentration distribution.

The expected similarities can be explicitly revealed through the following steps: recognizing that Π_{ij}^{SS} involves both elastic and osmotic stresses, we interpret the explicitly ϕ-dependent elastic stresses as an effective contribution to the osmotic pressure. Then, using the thermodynamic relationship between a free energy and osmotic pressure, we back out an 'effective' free energy density, $\Lambda(\phi, \Sigma_0)$, from the elastic terms.

In the first step, we have:

$$-\Pi_{yy}^{SS}(\phi_0, \Sigma_0) = \pi_{yy}^{os}(\phi_0) + \pi^{el}(\phi_0, \Sigma_0) \qquad (28)$$

$$\pi_{yy}^{os}(\phi_0) = \frac{1}{2}\phi_0^2 + \left(\frac{\bar{\xi}}{\bar{H}}\right)^2 \phi_0^{-3/2}\left[\phi_0 \frac{\partial^2 \phi_0}{\partial y^2} - \frac{5}{4}\left|\frac{\partial \phi_0}{\partial y}\right|^2\right]\left[\phi_0 \frac{\partial^2 \phi_0}{\partial y^2} - \frac{5}{4}\left|\frac{\partial \phi_0}{\partial y}\right|^2\right] \qquad (29)$$

$$\pi^{el}(\phi_0, \Sigma_0) = E\phi_0^{9/4}\Big[-\big(Q_{yy}^{SS}(\phi_0, \Sigma_0) - 1\big) + \frac{5}{8}\big(\mathrm{tr}\big(\boldsymbol{Q}^{SS}(\phi_0, \Sigma_0)\big) - 3 - \ln\big(\det\big(\boldsymbol{Q}^{SS}(\phi_0, \Sigma_0)\big)\big)\big)\Big] \qquad (30)$$

In the second step, we look back to the derivation of our two-fluid model and see that the osmotic pressure π and chemical potential μ are defined in terms of the free energy F as follows:

$$\frac{\partial \pi}{\partial y} = \phi \frac{\partial \mu}{\partial y} = \phi \frac{\partial}{\partial y}\frac{\delta F}{\delta \phi} \qquad (31)$$

When the local contribution to the osmotic pressure, $\pi_L^{os}(\phi)$, is known, one can invert (31) to solve for the corresponding value of the local (bulk) free energy of mixing $f_L(\phi)$:

$$\phi \frac{\partial^2 f_L}{\partial \phi^2} = \frac{\partial \pi_L^{os}}{\partial \phi} \qquad (32)$$

$$\frac{\partial}{\partial \phi}\left[\phi \frac{\partial f_L}{\partial \phi} - f_L\right] = \frac{\partial \pi_L^{os}}{\partial \phi} \qquad (33)$$

$$\frac{\partial f_L}{\partial \phi} + \left[-\frac{1}{\phi}\right] f_L = \frac{\pi_L^{os} - \pi_L^{os}(\phi_{ref})}{\phi} \qquad (34)$$

$$f_L(\phi) = \phi \int_{\phi_{ref}}^{\phi} d\phi' \left(\frac{\pi_L^{os}(\phi') - \pi_L^{os}(\phi_{ref})}{\phi'^2}\right) \qquad (35)$$

The value of ϕ_{ref} may be chosen arbitrarily (corresponds to a constant of integration, and the free energy is only defined to within a constant) so we typically choose $\phi_{ref} = 1$, corresponding to the homogeneous concentration of the solution.

Away from equilibrium, we propose the existence of $\mathcal{L}$ satisfying QTH, such that:

$$\frac{\partial}{\partial y}\left(\pi_{yy}^{os} + \pi^{el}\right) = \phi_0 \frac{\partial}{\partial y} \frac{\delta \mathcal{L}}{\delta \phi_0} \qquad (36)$$

If $\mathcal{L}$ satisfies QTH, then the above equation reduces to an expression for Λ (the flow-induced shift to the effective free energy) in terms of π^{el}:

$$\frac{\partial \pi^{el}}{\partial y} = \phi_0 \frac{\partial}{\partial y} \frac{\partial \Lambda}{\partial \phi_0} \qquad (37)$$

$$\frac{\partial \pi^{el}}{\partial \phi_0} = \phi_0 \frac{\partial^2 \Lambda}{\partial \phi_0^2} \qquad (38)$$

Integrating as before, we obtain:

$$\Lambda(\phi_0, \Sigma_0) = \phi \int_{\phi_{ref}}^{\phi} d\phi' \left(\frac{\pi^{el}(\phi', \Sigma_0) - \pi^{el}(\phi_{ref}, \Sigma_0)}{\phi'^2}\right) \qquad (39)$$

Thus, we have proven part (a) of wQTH by showing the existence of Λ satisfying QTH in the limit of high coupling friction. Specifically, we can now write equation (27) as:

$$\frac{\partial}{\partial \tau}\phi_0 = \frac{\partial}{\partial y}\left[M(\phi_0)\frac{\partial}{\partial y}\left[\frac{\delta \mathcal{L}}{\delta \phi_0}\right]\right] \qquad (40)$$

With $M(\phi_0) = \phi_0^{-1/2}$ and $\mathcal{L}$ defined in a manner consistent with equation (13).

$$\mathcal{L} = \bar{H}\int dy\ \left[f_L(\phi_0) + \Lambda(\phi_0, \Sigma_0) + f_{NL}\left(\phi_0, \frac{\partial \phi_0}{\partial y}\ldots\right)\right] \qquad (41)$$

The interested reader may wonder how the expression for $\Lambda(\phi_0, \Sigma_0)$ compares to the actual elastic free energy density of the system. In our two-fluid model derivation, we assume an elastic free energy density f^{el} from Rubber elasticity theory [33], such that in our dimensionless units:

$$f^{el}(\phi, \boldsymbol{Q}) = \frac{1}{2}E\phi^{9/4}(\mathrm{tr}(\boldsymbol{Q}) - 3 - \ln(det(\boldsymbol{Q}))) \qquad (42)$$

Thus, the elastic free energy density f^{el} is only indirectly related to the elastic contribution in $\mathcal{L}$, since ones choice of f^{el} determines the elastic stresses that appear in the momentum balances. Our analysis conclusively shows that SID in a two-fluid model does not minimize a quantity that is equivalent to the total free energy of the system.

4. Relationship Between the *O*(1) Asymptotic Equations and the Full 2-Fluid Model for 1D Shear Flows with a Constant Wall Shear Stress

The asymptotic limit of high coupling friction ($\bar{\xi} \gg 1$ for fixed $\bar{\xi}/\bar{H}$) may be a useful construct for demonstrating a relationship between model B and SID, but it is certainly not

representative of the real systems that our 2-fluid model is intended to describe ($\bar{\xi}\sim\varpi^{1/2} \ll 1$). Therefore, in this section, we seek to understand how the asymptotic model differs from the full model for $\bar{\xi}$ varying from the high friction limit to more realistic values of $\bar{\xi}\sim\varpi^{1/2}$. If part (b) of wQTH holds true, then the high coupling friction limit will still provide a meaningful qualitative description of the underlying physics for realistic coupling friction.

4.1. Linear Stability Results

To limit the scope of our investigation, we will be primarily concerned with studying the demixing instability that manifests in the range of $1 < Wi < \theta$, where the steady state shear stress depends weakly on the applied shear rate [13]. For this study, we choose the following set of material parameters to characterize a well-entangled semi-dilute polymer solution: $\theta = 120, E = 0.15, \varpi = 10^{-4}$. Unless otherwise specified, we choose a gap dimension of $\bar{H}/\bar{\xi} = 100$. For a more complete discussion of how each of these parameters qualitatively influences the system's linear stability to SID, the reader may refer to our previous work on the subject [13], and to related work by other authors [8]. In this section, we are primarily concerned with determining how the predictions of the asymptotic model differ from those of the full model.

We begin by considering the linear stability of the asymptotic and full models. We perform the linear stability analysis in the standard way, as outlined in our previous work [10]. Considering both the asymptotic model ($\bar{\xi} \gg 1$) and the full model (finite $\bar{\xi}$) we first assess the stability of the longest wavelength mode that fits in the system, $k = 2\pi$, and then test additional modes to determine whether the two models are in agreement with respect to the conditions

under which SID can be observed. Note that k has been non-dimensionalized by $1/H$ here, and $k = 2\pi$ is the longest wavelength mode that can be accommodated by our boundary conditions.

The stability of the asymptotic model can be determined from the corresponding model B, i.e. equation (40). The unstable window is locally bounded to a range of applied shear stresses, $0.60 < \Sigma_0 < 0.64$, corresponding to dimensionless strain rates of $3.2 < Wi < 11.5$ in the homogeneous base state. Within this unstable window, there is always a preferred (fastest growing) wavelength at which inhomogeneity will develop. In analogy with model B, very near the upper and lower limits of the unstable window, the $k = 2\pi$ mode is preferred, but shorter wavelengths are preferred in the interior of the unstable window. Furthermore, as with model B, the location of the stability boundary depends only on the ratio $\bar{\xi}/\bar{H}$, and not on the values of $\bar{\xi}$ and $\bar{H}$ independently.

By contrast, in the full model we find that the stability boundaries depend on $\bar{\xi}$ even for fixed values of $\bar{\xi}/\bar{H}$ (i.e. stability boundaries depend on the coupling friction). However, the dependence on $\bar{\xi}$ is extremely weak, and the numerical values of Σ_0 at the upper and lower bounds of the unstable window are in close (but not perfect) agreement with the asymptotic model; the stability boundaries only disagree at the fourth decimal digit in this case, and more generally to $\mathcal{O}(\varpi/\bar{H}^2)$, as we will soon show.

In the Figure 1 below, we plot the lower critical shear stress for linear instability, Σ_0^C, as a function of $\bar{\xi}$ for fixed $\bar{H}/\bar{\xi} = 100$. For large values of $\bar{\xi}$ (high coupling friction), Σ_0^C at the lower stability window converges to the limiting value predicted by the asymptotic model. As $\bar{\xi}$ decreases below 10^{-3}, a small departure is apparent, and a second asymptote is encountered for sufficiently small values of the coupling friction.

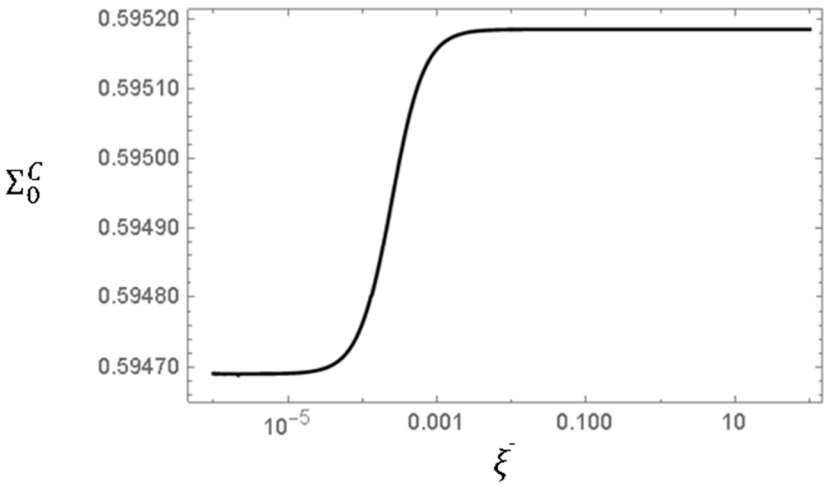

Figure 1: When the coupling friction is not asymptotically large (finite $\bar{\xi}$), the position of the system's neutral stability boundary is not entirely independent of the coupling friction. As an example, the figure above considers the lower critical shear stress for instability, Σ_0^C, as a function of $\bar{\xi}$ for fixed $\theta = 120, \varpi = 10^{-4}$, and $\bar{H}/\bar{\xi} = 100$. Here, we find that the unstable window becomes slightly broader with decreasing coupling friction (decreasing $\bar{\xi}$). This effect may be attributed to the loss of a stabilizing viscous contribution from the solvent, i.e. the friction is low enough for the polymer to shear band without having to force the solvent to shear band as well.

For an explanation of this change in the stability boundary, recall that lower values of $\bar{\xi}$ represent a reduced coupling friction in the present context. With a sufficiently weak coupling friction, the Newtonian solvent is free to retain a linear velocity profile irrespective of any demixing or shear banding of the polymer. Since the solvent's resistance to shear banding is stabilizing against SID, a reduced coupling friction (lower $\bar{\xi}$) lessens the solvent's influence and slightly broadens the range of Σ_0 for which demixing will occur. However, it is clear from Figure 1 that this effect is very weak.

If the governing equations of the full model are modified to prevent the two fluids from having different shear rates (i.e. $u_S = u_P$ for all conditions) then we find that the instability window no longer depends on the coupling friction at all (i.e. stability only depends on $\bar{\xi}/\bar{H}$). Considering equation (3) we see that the characteristic scale of the difference between u_S and u_P goes as:

$$u_S - u_P \sim \frac{1}{\bar{H}^2}\frac{\partial \Pi_{xy}}{\partial y} \sim \frac{\varpi E}{\bar{H}^2}\frac{\partial^2 u_S}{\partial y^2} \sim \mathcal{O}\left(\varpi E\left(\frac{k}{\bar{H}}\right)^2\right) \qquad (43)$$

Thus, the unstable window of the $k = 2\pi$ mode in the asymptotic model and the full model differ by $\mathcal{O}(E\varpi/\bar{H}^2)$. For $\bar{H} = 1$, as considered here, we have seen that the asymptotic model offers a good prediction of the neutral stability boundary (accurate to $\mathcal{O}(\varpi)$, where $\varpi = 10^{-4}$ in this case) but any disagreement between the two becomes vanishingly small in the macroscopic limit, represented asymptotically by $\bar{H} \gg 1$ and fixed $\bar{\xi} \sim \varpi^{1/2}$.

Although the full model and the toy model agree with respect to the stability boundary of $k = 2\pi$ perturbations, it is not necessarily true that the broadest window of instability is determined by the $k = 2\pi$ mode (as is predicted by the asymptotic model). In other words, to establish full agreement with respect to the boundaries of linear stability, we must confirm that there are no experimentally relevant situations for which a $k = 2\pi$ perturbation is stable but a $k > 2\pi$ perturbation is unstable.

As an example, we consider the same set of material parameters but for a larger system, $\bar{H}/\bar{\xi} = 10^4$, and a much lower coupling friction ($\bar{\xi} = 10^{-4} \ll \varpi^{1/2}$). Setting Σ_0 to a value that is intermediate to the limiting unstable Σ_0 at low/high coupling friction (e.g. $\Sigma_0 = 0.595$ in Figure 1), we find that the system is only unstable to perturbations of $k = 2n\pi$ with $n = 25 -$

122. Returning to the analysis of equation (43), we see that the stabilizing contribution of the solvent viscosity is lost when $k^2 \sim \bar{H}^2/\varpi$, coinciding with the lower bound of unstable k values. The upper end of the unstable range is set by a resistance to forming concentration gradients on length-scales below the solution correlation length, $k \sim \mathcal{O}(\bar{H}/\bar{\xi})$.

In this example, we have allowed an unphysically low coupling friction, and the intrusion of unstable modes at short wavelength should be considered likewise unphysical. For realistic values of the coupling friction, $\varpi \sim \bar{\xi}^2$, the wavelength at which solvent effects are lost should be the same as the wavelength at which interfacial stresses become dominant, $k^2 \sim \bar{H}^2/\bar{\xi}^2$. Furthermore, the loss of solvent viscous stabilization should generally be negligible $\mathcal{O}(\varpi)$ compared to the $\mathcal{O}(1)$ stabilizing effect that emerges from interfacial stresses, so in our view there is no physical basis to argue that short wavelength modes can be unstable while longer wavelength modes are not.

Overall, it seems that for any physically reasonable treatment of the coupling friction and the interfacial stresses, the $k = 2\pi$ mode should always have the broadest unstable window. Furthermore, because the full model and the asymptotic model agree on the $k = 2\pi$ stability boundary for macroscopic systems, the asymptotic model and the full model are in agreement with respect to the linear stability boundaries of SID.

Finally, it is worth noting that migration induced stress, which is absent in the asymptotic model but present in the full model, has no influence on the absolute stability of the system. When the rate of mass transport is slow (as is true at a neutral stability boundary), the viscoelastic forces from migration induced stress are predominantly viscous. These viscous stresses can attenuate – but never reverse – the velocity of migration within the system.

4.2. Simulations and Nonlinear Dynamics for 1D Shear Flows with Constant Wall Shear Stress

Now, for conditions that fall within the unstable window, we numerically solve the full model and the asymptotic model for a range of $\bar{\xi}$, spanning values that are realistic ($\bar{\xi}\sim\varpi^{1/2}$) to unrealistic, but relevant to the asymptotic model ($\bar{\xi} \gg 1$). By means of these simulation results, we confirm qualitative agreement of SID dynamics across all values of $\bar{\xi}$.

For a macroscopic system with realistic coupling friction, $\bar{H} \gg 1, \bar{\xi}\sim\varpi^{1/2}$, we have shown that the full model and asymptotic model are in quantitative agreement with respect to the values of Σ_0 for which there exists a linear instability to SID. In this section, we will show that there is also qualitative agreement in the non-linear dynamics that follow the initial demixing instability. In particular, we show that for a range of $\bar{\xi}$, there are coarsening dynamics and inhomogeneous steady states in the full model that directly correspond to the coarsening dynamics and inhomogeneous steady states predicted by the asymptotic model (and thus also model B).

The transient evolution of velocity and concentration profiles during demixing has been discussed in detail in our previous work [10] [13]. We will summarize some of that work here, but in the interest of concise exposition, we will primarily focus only on (1) changes in scalar metrics of inhomogeneity and (2) the final concentration profile at steady state. For a metric of the overall departure from a uniform concentration, we use the L2 norm of $\phi - 1$:

$$L_2\phi = \left[\int_0^1 dy\,(1-\phi)^2\right]^{1/2} \qquad (44)$$

One might also want to consider the extent to which a departure from global homogeneity involves regions where the concentration profile is varying in space. For this, we consider a local metric of inhomogeneity, based on the L2 norm of $\nabla\phi$:

$$L_2\nabla\phi = \left[\int_0^1 dy \left(\frac{\partial\phi}{\partial y}\right)^2\right]^{1/2} \qquad (45)$$

In Figure 2, we see that during the initial linear growth of inhomogeneity, both $L_2\phi$ and $L_2\nabla\phi$ are increasing. In the terminal stages of demixing, both of these metrics begin to saturate. Shortly thereafter, coarsening processes reduce the number of interfaces, which leads to infrequent and abrupt increases in $L_2\phi$ with a matching decrease in $L_2\nabla\phi$. This process continues until only two interfaces remain within the system (the minimum number that will satisfy periodic boundary conditions).

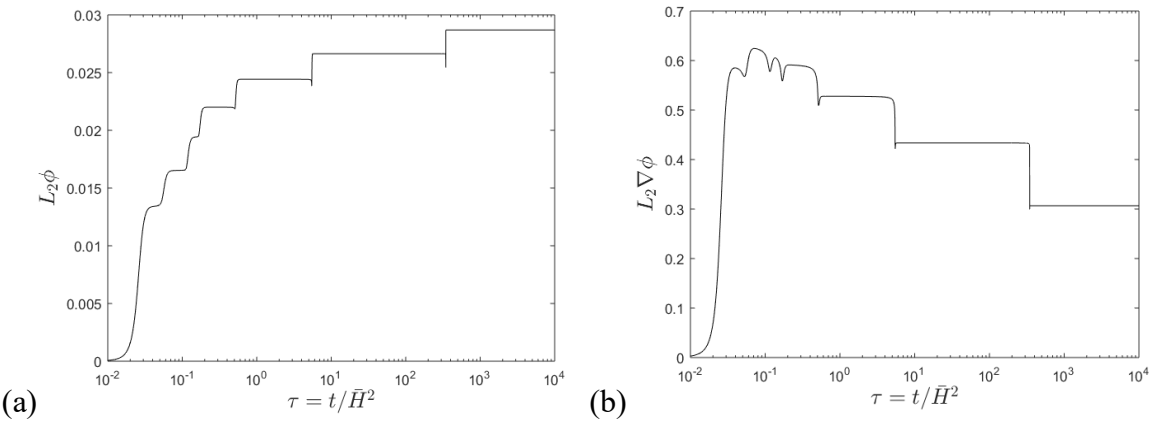

Figure 2: Illustrating the growth of global (a) and local (b) inhomogeneity during the course of a SID instability. These simulations consider start-up flow of the asymptotic model (equations (17) - (23)) for $\theta = 120, E = 0.15, \varpi = 10^{-4}, \bar{H}/\bar{\xi} = 100$, and $\Sigma_0 = 0.6225$. The imposed shear stress would correspond to $Wi \approx 7$ for this system in homogeneous flow conditions. Simulations begin from an initial concentration profile that is mostly homogeneous except for a small, $\mathcal{O}(10^{-5})$ perturbation of random Gaussian noise. At short times, $\tau < 0.1$, both measures of inhomogeneity are increasing in time. At longer times, $\tau > 0.1$, the global metric (a) continues to increase while the local metric (b) begins to decrease with step-like changes. These step-like changes correspond to coarsening events wherein the system reduces the number of interfaces that it contains.

In Figure 3- Figure 5 below, we provide snapshots of the concentration profile at relevant times for the simulation represented in Figure 2. These simulations correspond to solutions of the asymptotic model with $= 120, E = 0.15, \varpi = 10^{-4}, \bar{H}/\bar{\xi} = 100$, deformed at $\Sigma_0 = 0.6225$ (corresponding to $Wi \approx 7$ in the associated homogeneous state). As an initial condition, the polymer conformation tensor is assumed to be at rest ($\boldsymbol{Q} = \boldsymbol{I}$) and a small amount of random Gaussian noise is applied to the concentration profile.

For the purposes of this work, we define the transition from spinodal decomposition to coarsening as the time at which $L_2 \nabla \phi$ is globally maximized, here occurring roughly around $\tau = 0.10$. The concentration profile at this time is provided in Figure 3. At $\tau = 0.1$, the system has selected a preferred (fastest growing) wavelength for inhomogeneity, and as the amplitude saturates, coarsening begins. Typically it is the narrowest peaks/valleys that vanish first (in this case, the peak near $y = 0.55$).

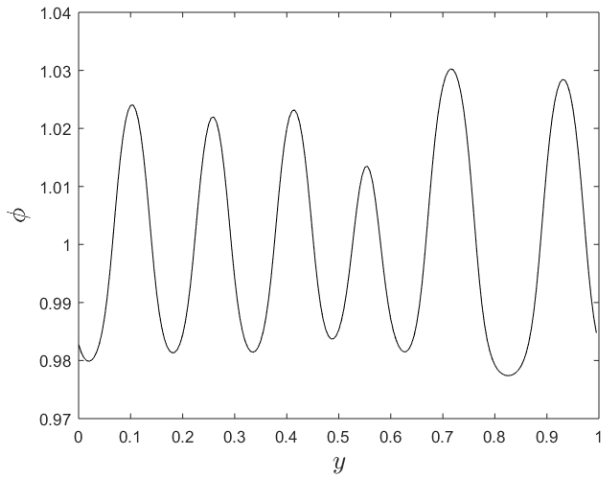

Figure 3: Snapshot of the polymer concentration profile, taken at $\tau = 0.1$ after start-up. These simulations consider start-up flow of the asymptotic model (equations (17) - (23)) for $\theta = 120, E = 0.15, \varpi = 10^{-4}, \bar{H}/\bar{\xi} = 100$, and $\Sigma_0 = 0.6225$. Beginning from an initial condition of small amplitude random Gaussian noise, the system has selected a preferred (fastest growing) mode. The perturbation is now roughly sinusoidal with wavenumber $k = 10\pi$.

At $\tau = 1$, the system has undergone several coarsening steps; the average spacing between interfaces has increased, and we can clearly see an early indication of saturated amplitudes in the concentration profile (in this case, most evident around $y = 0.9$):

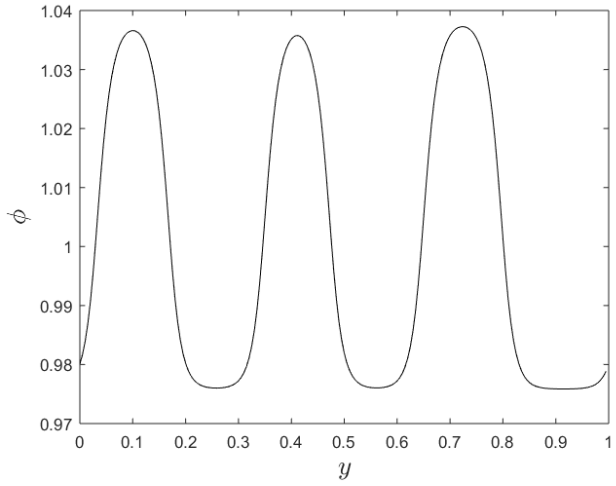

Figure 4: Snapshot of the concentration profile at $\tau = 1.0$ after start-up. Comparing to Figure 3, we see that there are fewer bands (and fewer interfaces) than before. These simulations consider start-up flow of the asymptotic model (equations (17) - (23)) for $\theta = 120, E = 0.15, \varpi = 10^{-4}, \bar{H}/\bar{\xi} = 100$, and $\Sigma_0 = 0.6225$.

Each coarsening step becomes successively slower than the last, but by $\tau = 1000$, we observe the final coarsening step possible for our present system size. At this point, only two interfaces remain:

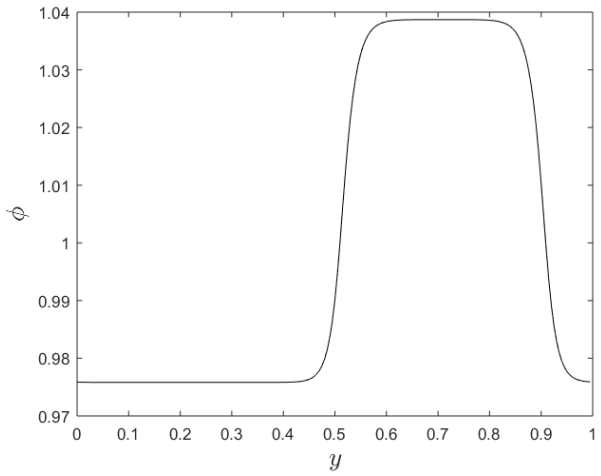

Figure 5: steady state concentration profile ($\tau = 10^4$). Comparing to Figure 3 and Figure 4, we see that the system has continued to coarsen, eliminating interfaces until there are only two remaining (the minimum number possible for periodic boundary conditions). These simulations consider start-up flow of the asymptotic model (equations (17) - (23)) for $\theta = 120, E = 0.15, \varpi = 10^{-4}, \overline{H}/\bar{\xi} = 100$, and $\Sigma_0 = 0.6225$.

The preceding simulation was performed using MatLab's ode15s solver, $N = 200$ grid points, and Fourier collocation for computing spatial derivatives. The spatial resolution provides $\sim$20 grid points per interface, which yields a solution that is spatially and temporally converged. However, with $N = 100$ ($\sim$10 grid points per interface) the system encounters a locally stable stationary solution that is not completely coarsened (coarsening is arrested prematurely). In this case, we have found that there is a modest (though perhaps initially surprising) constraint on the spatial resolution required for fully converged dynamics. Demands on spatial resolution becomes more problematic for larger systems, in which the coarsening dynamics become increasingly slow. This is therefore a salient example where analytic results from the model B literature are quite valuable: from the model B literature, we know that any incompletely coarsened stationary state must be unstable, and the average domain size grows very slowly [23].

Next, we compare the simulation results of the asymptotic model with the full model for $\bar{\bar{\xi}} = 0.01, 0.1,$ and 1. In each case, we initialize the system from the same random seed that was used for the preceding simulations results described for the asymptotic model. For the largest value, $\bar{\bar{\xi}} = 1$, the results are nearly indistinguishable from the asymptotic model ($\bar{\bar{\xi}} \gg 1$). For the smaller value of $\bar{\bar{\xi}} = 0.01$, however, we see a significant departure at short times. The departure at short times can be explained in terms of the effects of migration-induced strain on the selection (and growth rate) of the preferred wavelength for demixing.

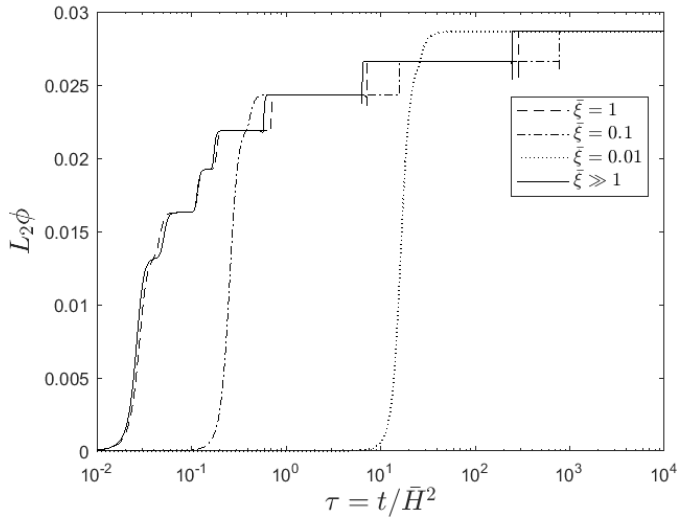

Figure 6: comparing the global metric of inhomogeneity during the course of start-up for the asymptotic model, and for the full model across a range of coupling frictions. These simulations consider start-up flow of the asymptotic model (equations (17) - (23)) for $\theta = 120, E = 0.15, \varpi = 10^{-4}, \bar{H}/\bar{\bar{\xi}} = 100$, and $\Sigma_0 = 0.6225$. For the largest value of $\bar{\bar{\xi}} = 1$, we find that the asymptotic model and the full model are nearly indistinguishable from one another. With decreasing coupling friction, however, the onset of demixing is increasingly delayed to longer times in τ. We attribute this delay to migration induced stress causes the system to demix with a longer preferred wavelength and a slower overall growth rate. After the initial spinodal period, however, the coarsening dynamics tend to look similar across all values of $\bar{\bar{\xi}}$ considered.

Similar trends are observed in a comparison of $L_2\nabla\phi$ for all four cases. We have also compared the steady state concentration profiles for the four cases in terms of the maximum and minimum values of ϕ that appear within the system. In all four models, the maximum and

minimum concentrations are in agreement to at least four decimal digits; the maximum and minimum values are around $\phi = 1.04$ and $\phi = 0.98$, respectively. For the range of $\bar{\xi}$ considered here, there is a small $\mathcal{O}(\varpi)$ disparity in the steady state concentration due to the fact that the asymptotic model does not account for differences in the polymer and solvent shear rate across the interface between shear bands.

Overall, the numerical simulations provide evidence that the late stages of coarsening are similar for the full model and the asymptotic model over the range of conditions considered. Since we know that the asymptotic model (and model B) never show arrested coarsening at long times, it is reasonable to expect that the full model will follow the same behavior.

If future studies encounter arrested coarsening in simple shear flow (excluding attribution to inadequate spatial resolution) we speculate that the most likely underlying cause would be related to differences in the polymer and solvent shear rate across the interface between bands. For the moment, however, arrested coarsening seems like an unlikely scenario. We argue that the $\mathcal{O}(\varpi)$ effects of the solvent primarily serve to encourage a more linear velocity profile. Coarsening events decrease the number of interfaces (where the velocity profile is locally non-linear), and so we speculate that any $\mathcal{O}(\varpi)$ effects neglected by the asymptotic model will only serve to encourage coarsening rather than arrest it.

5. Using the Lyapunov Functional to Obtain New Results

In section 3 of this paper, we proved part (a) of wQTH: in the asymptotic limit of high coupling friction, the leading order dynamics of SID in our two-fluid system are equivalent to the dynamics of a model B phase separation. Then, in sections 4.1 and 4.2 of this work, we

presented evidence that part (b) of wQTH holds as long as the coupling friction is not reduced below values that are experimentally attainable, $\bar{\xi} \sim \varpi^{1/2}$, and as long as the system can be considered macroscopic, $\bar{H} \gg 1$. Under such conditions, the asymptotic model predicts stability boundaries with vanishingly small errors, $\mathcal{O}(\varpi/\bar{H}^2)$. After the onset of a demixing instability, we also find that the subsequent non-linear dynamics are in qualitative agreement, and the eventual steady states are in quantitative agreement to $\mathcal{O}(\varpi)$. At this point, we remind the reader that we have only demonstrated these results for the case of simple shear flows driven by a constant applied stress.

In many respects this work only serves to confirm what a number of researchers have long suspected, namely that SID in a two-fluid model is indicative of a flow-induced change in the potential responsible for mixing/demixing phenomena [1] [34] [28] [11] [35]. But now, we can properly quantify that change in terms of $\Lambda(\phi, \Sigma_0)$. In this section, we compute the Lyapunov functional $\mathcal{L}$ in terms of an effective bulk free energy density $f_\Lambda = f_L + \Lambda$ in the limit of $\bar{\xi}/\bar{H} \ll 1$. We then use tools from equilibrium thermodynamics to analyze the local and global stability of both homogeneous and inhomogeneous steady states for different values of Σ_0.

In the limit of a macroscopic system, $\bar{\xi}/\bar{H} \ll 1$, we are primarily interested in comparing homogeneous steady states and fully coarsened inhomogeneous steady states (since all other steady states are known to be unstable). For such systems, one can approximate the concentration profile as two locally homogeneous regions of concentrations ϕ^I and ϕ^{II} connected by an interface of width $\mathcal{O}(\bar{\xi}/\bar{H})$. For a fully homogeneous system, $\phi^I = \phi^{II}$.

When computing $\mathcal{L}$ or F for such a system, any contribution from the narrow interface can be neglected to leading order, so that the relevant potential is only dependent on the state of the system in the extended locally homogeneous regions:

$$\mathcal{L}/\overline{H} = y^I f_\Lambda(\boldsymbol{\phi}^I, \Sigma_0) + y^{II} f_\Lambda(\boldsymbol{\phi}^{II}, \Sigma_0) + \mathcal{O}(\bar{\xi}/\overline{H}) \qquad (46)$$

where y^I is the volume fraction of the system at $\boldsymbol{\phi}^I$ and $y^{II} = 1 - y^I$ is the volume fraction of the system at $\boldsymbol{\phi}^{II}$. Furthermore, y^I is related to $\boldsymbol{\phi}^I$ and $\boldsymbol{\phi}^{II}$ by the conservation of mass equation (lever rule):

$$\boldsymbol{\phi}^I y^I + \boldsymbol{\phi}^{II}(1 - y^I) = 1 \qquad (47)$$

Most importantly, there is only a finite set of admissible values for $\boldsymbol{\phi}^I$ and $\boldsymbol{\phi}^{II}$ at any given Σ_0. As a first constraint on $\boldsymbol{\phi}^I$ and $\boldsymbol{\phi}^{II}$, the polymer normal stress in the gradient direction must be equal in each of the two bands to ensure that no further changes in concentration occur:

$$\Pi^{SS}_{yy}(\boldsymbol{\phi}^I, \Sigma_0) = \Pi^{SS}_{yy}(\boldsymbol{\phi}^{II}, \Sigma_0) \qquad (48)$$

A second, more subtle, constraint is that there must exist a valid solution for the interface connecting the two locally homogeneous regions (i.e. the polymer normal stresses and shear stresses must be balanced across the interface). For these kinds of problems, one often has to solve an 'inner solution' that resolves the interface and uniquely determines the 'outer solution' (composition of bulk phases) via a matching condition. The correct outer solution is the one that matches the inner solution far from the location of the interface.

One cannot usually obtain the matching condition without solving the entire inner solution, but this case presents a fortunate exception to that rule. To satisfy a matching constraint, the inner solution must become free of concentration gradients (locally homogeneous) very far from

the interface. With this constraint in mind (and an appropriate integrating factor) the governing equations of the inner solution can be integrated to obtain a constraint on ϕ^I and ϕ^{II} [36]:

$$0 = \int_{\phi^I}^{\phi^{II}} d\phi \left[\frac{\Pi_{yy}^{SS}(\phi, \Sigma_0) - \Pi_{yy}^{SS}(\phi^I, \Sigma_0)}{\phi^2} \right] \qquad (49)$$

The two constraints (48) and (49) on ϕ^I and ϕ^{II} can be equivalently represented as a common tangent construction on the effective free energy density, f_Λ, wherein the effective osmotic pressure π_Λ and the effective chemical potential μ_Λ must be balanced between the two shear bands:

$$\mu_\Lambda = \frac{\partial f_\Lambda}{\partial \phi} \qquad \pi_\Lambda = \phi \mu_\Lambda - f_\Lambda \qquad (50)$$

Equation (48) is equivalent to $\pi_\Lambda(\phi^I) = \pi_\Lambda(\phi^{II})$ and equation (49) is equivalent to $\mu_\Lambda(\phi^I) = \mu_\Lambda(\phi^{II})$. This can be contrasted with the selection rule proposed by Jou et. al., in which a Gibbs free energy was assumed (but not proven) to be the relevant minimized quantity (see equations (6.12), (6.32-34), (6.79) in Jou et. al., 2011 [35]).

With these constraints on the steady banded solutions, there are only a finite set of states (defined in terms of band compositions ϕ^I and ϕ^{II}) for which $\mathcal{L}$ may be computed at a given Σ_0.

For a first case, we consider a shear flow where the polymer is not substantially deformed from its equilibrium conformation, $\Sigma_0 = 0.01$ ($Wi = 0.01$ in the homogeneous base state). For this flow, we plot f_Λ versus ϕ in Figure 7. We see that f_Λ is a globally convex function of ϕ, so no inhomogeneous steady states exist (i.e. there is no line of common tangents that can produce a lower free energy state), and so the homogeneous steady state is necessarily globally stable:

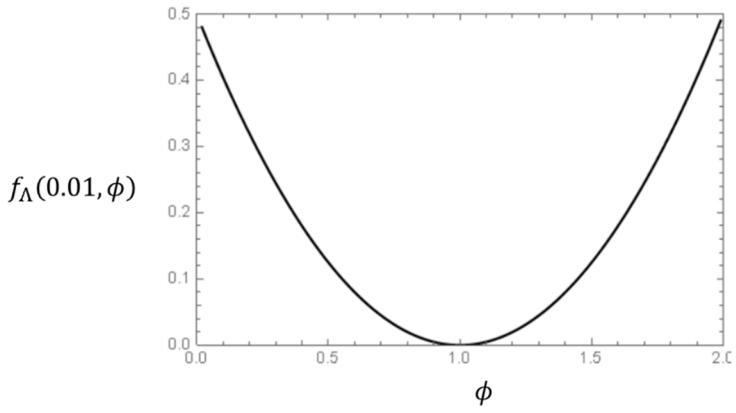

Figure 7: Graphical representation of the global stability of a homogeneous steady state for low rates of deformation. The effective free energy density, f_Λ, is a globally convex function of ϕ for $\Sigma_0 = 0.01$ given $\theta = 120, E = 0.15, \varpi = 10^{-4}$ and $\bar{H}/\bar{\xi} \gg 1$. As such, the system only possesses a single steady state conformation (homogenous flow) and this conformation is not susceptible to SID.

For stronger deformations, the system approaches a neutral stability boundary near $\Sigma_0 = 0.60$. In the asymptotic model (as in model B) one must consider the existence of finite amplitude instabilities, where phase separation occurs via a mechanism of nucleation and growth as opposed to spinodal decomposition. Here, we consider $\Sigma_0 = 0.59$ (corresponding to $Wi = 3$ in the homogeneous base state). For small departures from homogeneity (i.e. $\phi = 1$), f_Λ is locally convex, and therefore the homogeneous base state is stable to disturbances of sufficiently small amplitude. However, as shown in Figure 8, over a wider range of ϕ we find that f_Λ has a double-well structure that indicates the existence of an inhomogeneous steady state:

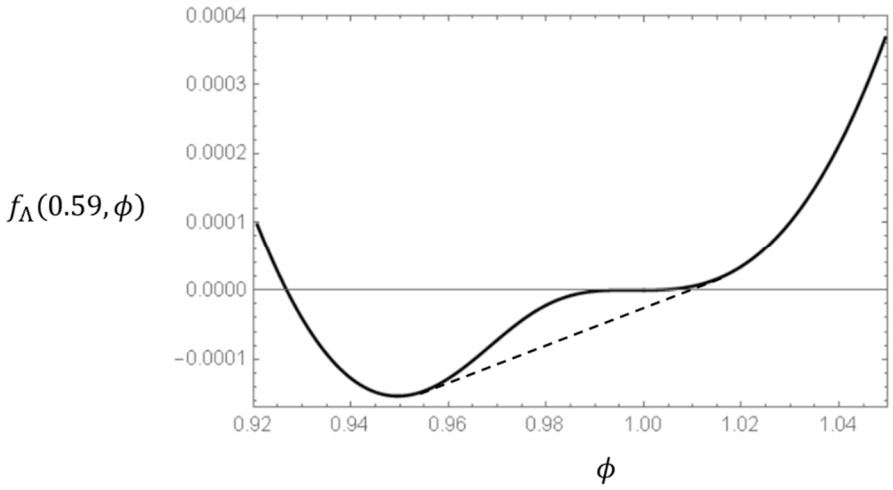

Figure 8: Graphical representation of the global stability of a homogeneous steady state for low rates of deformation for $\Sigma_0 = 0.59$ given $\theta = 120, E = 0.15, \varpi = 10^{-4}$ and $\bar{H}/\bar{\xi} \gg 1$. The effective free energy landscape is locally convex about $\phi = 1$, indicating that the homogeneous state is locally stable to sufficiently small amplitude perturbations. However, a common tangent line reveals the existence of a shear banded solution that is more stable.

By eye, one may apply a common tangent construction to see that the compositions in the locally homogeneous regions are around $\phi^I = 0.95$ and $\phi^{II} = 1.01$. For this shear banded state, $\mathcal{L}/\bar{H} = -2.3 \cdot 10^{-5}$ which is lower than the value $\mathcal{L} = 0$ for the homogeneous state. Thus, a numerical simulation of this system with stochastic forcing by thermal noise should eventually show demixing that proceeds via nucleation and growth. As an inexpensive substitute for a full stochastic study of nucleation in the full model (finite $\bar{\xi}$), we apply a relatively large amplitude perturbation to the concentration at $t = 0$ and observe its subsequent evolution. The perturbation $\delta\phi$ crudely approximates a square wave, in keeping with the approximation of equation (46):

$$\delta\phi = 10^{-2} \tanh\left(5 \cos\left(2\pi\left(y - \frac{1}{2}\right)\right)\right) \qquad (51)$$

This perturbation is applied at $t = 0$ and a constant shear stress of $\Sigma_0 = 0.59$ is enforced thereafter. The evolution of the concentration profile is given in the figure below. At short

times, the perturbation decays because it is not optimally shaped for nucleation. At longer times, the concentration profile begins to form a clear 'crease' at its minimum value, indicating the nucleation of a high shear band. The nucleated band grows until it eventually saturates and broadens to reach the final inhomogeneous steady state predicted by the common tangent construction.

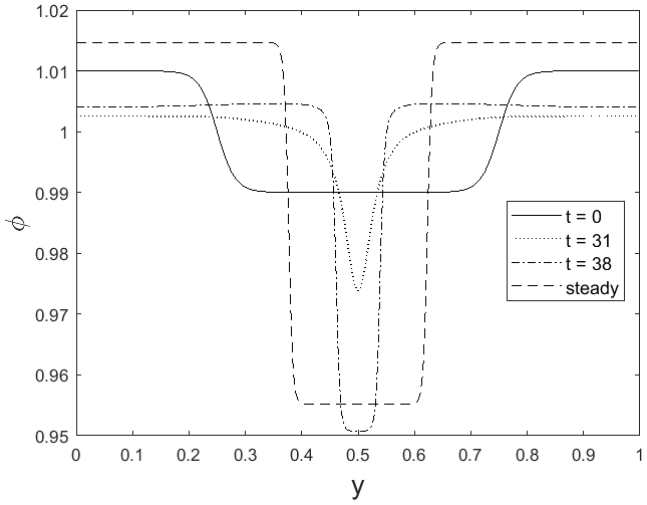

Figure 9: Snapshots of the concentration profile during the course of nucleation and growth of a shear band from a finite amplitude initial perturbation. For a system of $= 120, E = 0.15, \varpi = 10^{-4}$ and $\bar{H}/\bar{\xi} = 100$, we apply a sustained deformation of $\Sigma_0 = 0.59$. Under these conditions, the system is linearly stable when homogeneous, but a sufficiently large amplitude perturbation will push the system towards a (preferred) shear banded state. At short times, our perturbation appears to decay, but a low-concentration band is successfully nucleated, causing the perturbation to grow at longer times. At steady state, the system is banded, as predicted by the analysis supporting Figure 8.

Similar sub-critical instabilities will exist all the way down to $\Sigma_0 = 0.57$ ($Wi = 2.25$), which is the lowest Σ_0 for which an inhomogeneous steady state exists in the stress plateau region. These nucleation events have been observed in simulations previously: for example, Cromer et. al. observed that banded and homogeneous steady states were both possible from the same initial condition, depending on whether the deformation protocol involves a fast or slow ramp to the target deformation rate [10]. This ramp-rate dependence was initially attributed to transient

enhancement of the instability during stress overshoot, but a simpler explanation seems more likely now: a perturbation that is large enough to nucleate a demixing event may survive through the transients of a rapid start-up protocol, but will trivially decay by diffusion for a slow start-up protocol.

Finally, under the same conditions ($\Sigma_0 = 0.59$), we evaluate f_Λ over an even broader window to determine whether any other inhomogeneous steady state could be more favorable than the steady state observed in Figure 8. In fact, we find that such a state does exist:

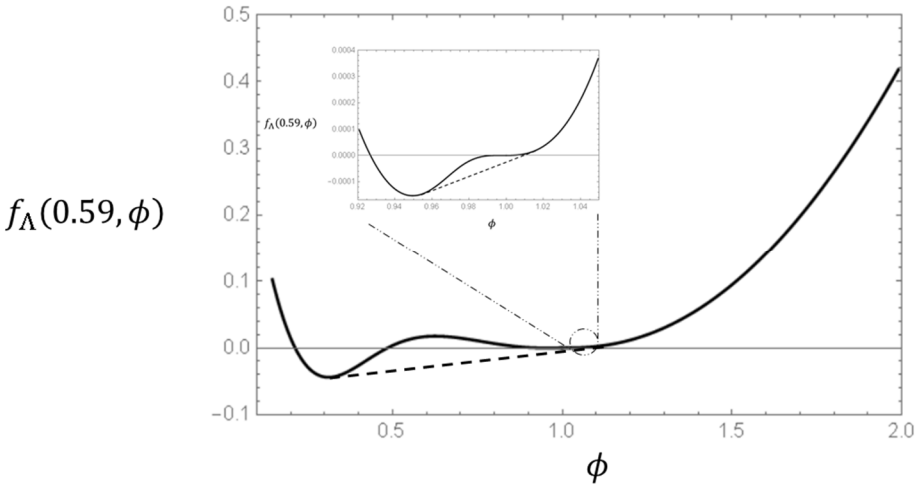

Figure 10: Graphical representation of the global stability of a homogeneous steady state for low rates of deformation for $\Sigma_0 = 0.59$ given $\theta = 120, E = 0.15, \varpi = 10^{-4}$ and $\bar{H}/\bar{\xi} \gg 1$. This is an expanded view of the analysis contained in Figure 8 (inset). The shear banded concentration profile of Figure 8 and Figure 9 is locally stable but still susceptible to nucleation of a band with even lower concentration.

By eye, one can apply a common tangent construction to see that the compositions in the locally homogeneous regions are around $\phi^I = 0.3$ and $\phi^{II} = 1.1$. For this state, $\mathcal{L}/\bar{H} = -4.8 \cdot 10^{-3}$, which is even more negative (and therefore more stable) than the inhomogeneous steady state represented in Figure 8 and Figure 9. Whereas the shear banded steady state from that case is associated with the unstable window in the stress plateau (as has been the primary focus of this

paper) this second shear banded steady state corresponds to an inhomogeneous steady states that one would usually encounter via the *linear* instability window at high Wi (as discussed in our previous work [13]). To the extent that the two-fluid model provides a faithful representation of SID in semi-dilute polymer solutions, this means that there could be conditions under which a linear instability leads to SID in the stress plateau and then, at much later times, a secondary SID event will nucleate and grow in a low-ϕ domain.

The construction of so-called 'flow-phase diagrams' in analogy to the spinodal/binodal phase diagrams of model B is an interesting exercise, and we refer the interested reader to earlier work by Fielding and Olmstead for a more complete discussion [7]. The flow-phase diagrams that we find for our model are qualitatively similar to what has already been reported there. As an example, we present a flow-phase diagram for our system below ($\theta = 120, \varpi = 10^{-4}, E = 0.15, \bar{\xi}/\bar{H} \gg 1$ for $\phi = \phi_o$). The dashed line corresponds to the boundary of linear stability (spinodal) while the solid curve corresponds to the set of coexisting shear bands (binodal). The dotted contours corresponding to the homogeneous constitutive curves for $\phi/\phi_0 = 0.9, 1,$ and 1.1 are superimposed on the flow phase diagram for added context. Note that the unstable window intersects the homogeneous constitutive curve for $\phi = \phi_o$ at shear stresses around $\Sigma_0 \sim 0.62$ and $Wi \sim 3 - 10$, and shear banded steady states can be observed between $Wi \sim 2$ and $Wi \sim 20$.

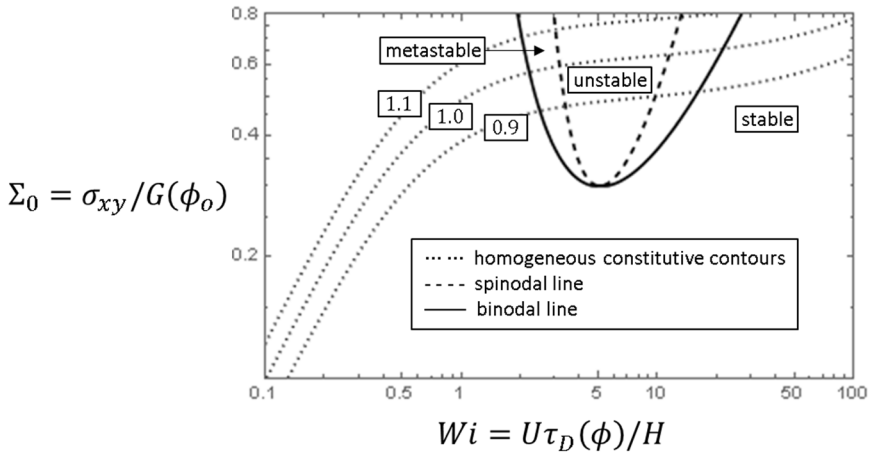

Figure 11: The flow phase diagram for a system with $\theta = 120, E = 0.15$, and $\varpi = 10^{-4}$ at absolute polymer volume fraction $\phi = \phi_o$. On the vertical axis, we plot the shear stress, Σ_0, which is the absolute shear stress normalized by the shear modulus of a homogeneous system with concentration ϕ_o. On the horizontal axis, we plot the Wi corresponding to homogeneous flow, where the relaxation time $\tau_D(\phi)$depends on the polymer concentration. The dotted lines represent homogeneous constitutive curves for $\phi/\phi_o = 1.1, 1.0$ and 0.9. Note that varying the ratio of ϕ/ϕ_o mostly shifts the homogeneous constitutive curve vertically relative to the 'spinodal' and 'binodal' boundaries of our flow phase diagram.

Consistent with earlier findings, we observe a lower critical concentration for shear induced demixing of semi-dilute entangled polymer solutions. For more concentrated solutions (beyond the capabilities of our semi-dilute model) an upper critical concentration for shear induced demixing must exist as well, since SID cannot occur in the pure melt state.

As a closing discussion on this section, we make a final note that the Lyapunov stability analysis presented here is ultimately derived from a force balance on the constituent fluids. We have not assumed (nor have we found) that the system demixes to minimize its free energy or maximize/minimize its entropy production.

Having investigated flows with constant imposed shear stress, we will briefly consider some more surprising results that emerge when these same methods of analysis are applied to seemingly similar flow protocols. First, we look at the case of simple steady shear flows driven

by a constant wall velocity, and second, we consider the problem of large amplitude oscillatory shear flows (LAOS) driven by periodic oscillations of the boundary shear stress.

6. Steady simple shear with constant wall velocity

A consideration of shear flows driven by a constant boundary velocity turns out to be much more difficult because it introduces a second conserved variable in addition to concentration. Repeating the same derivation of an asymptotic model in the limit of high coupling friction, we obtain a final set of equations:

$$\frac{\partial}{\partial t}\phi_0 = \frac{\partial}{\partial y}\left[M(\phi_0)\frac{\partial}{\partial y}\left[\frac{\delta \mathcal{L}}{\delta \phi}\right]_{\Sigma_0}\right] \qquad (52)$$

$$\int dy\, \dot{\gamma}_S(\Sigma_0, \phi_0) = Wi \qquad (53)$$

Note that here $\mathcal{L}[\phi_0, \Sigma_0]$ is still defined as in equation (41), but the shear stress Σ_0 is no longer constant in time. Instead, the shear stress changes in response to changes in the whole concentration profile (Σ_0 is a functional of ϕ_0 and Wi).

One might intuit that shear stress and shear rate are conjugate variables (like pressure/volume, temperature/entropy, or stress/strain in an elastic solid) and that a Legendre transformation would yield a Lyapunov functional for the conserved shear rate case. However, it turns out that there is already a family of variables conjugate to shear stress, none of which is equivalent to the Weissenberg number. The conjugate variables to shear stress, $\hat{S}$, have the form:

$$\hat{S} = -\left(\frac{\partial \mathcal{L}}{\partial \Sigma_0}\right)_{\phi} + g(\Sigma_0) \neq Wi \qquad (54)$$

where $\mathcal{L}$ is the Lyapunov functional for constant shear stress and $g(\Sigma_0)$ is an arbitrary function of Σ_0. Thus, a naïve attempt at a Legendre transformation ($\hat{\mathcal{L}} = \mathcal{L} - Wi\Sigma_0$) does not yield a potential that is minimized when the shear rate is conserved. It may be possible to find a Lyapunov functional for the problem of SID at constant Wi, but our efforts to that end have so far proven fruitless.

Nonetheless, it turns out that all linear stability results from the constant shear stress case transfer to the case of constant overall shear rate. Under constant shear stress conditions, one can show that for a linear instability to demixing (homogeneous steady states) or a linear instability to coarsening (inhomogeneous steady states) the overall shear rate does not change to linear order. The shear rate increases where the concentration decreases (and vice versa) such that, to linear order, the conservation of concentration implies a conservation of shear rate. Thus, whatever makes the system unstable at constant stress will also make the system unstable at constant shear rate.

Likewise, the equations used to predict shear banded steady states at constant applied stress can also be used to predict steady states at constant shear rate. The shear stress Σ_0 must be treated as an additional unknown but the 'conservation of shear rate' presents an additional constraint so that the problem remains well-posed:

$$\dot{\gamma}_S(\Sigma_0, \phi^I)y^I + \dot{\gamma}_S(\Sigma_0, \phi^{II})y^{II} = Wi \qquad (55)$$

So far, there is no evidence (whether from simulations or experiments) to suggest that the metastable branch of homogeneous solutions under constant shear stress conditions will behave qualitatively differently under constant boundary velocity conditions. For shear banding wormlike micelles, there is experimental evidence showing no practical difference between the

two choices of boundary conditions [37], and so it may be worthwhile to repeat this experimental study for SID in polymer solutions.

7. Large Amplitude Oscillatory Shear Flows

In this final section, we will consider the problem of SID in large amplitude oscillatory shear (LAOS) flows. In previous works [10] [13], we have considered the ways in which SID phenomena manifest in practical experimental geometries, with Couette flow as the primary focus. However, while Couette flows are well-suited for experimental study of shear induced migration in general, they are not ideally suited for studying the most fundamental aspects of SID. Macroscopic stress gradients make it difficult to isolate a dominant cause of polymer migration, and curved streamlines can introduce elastic instabilities that disrupt a 1D idealization of the flow. Experimental interest in LAOS flows is also growing [38] [39], and so we suggest that planar LAOS may be a better choice for future studies of SID phenomena in semidilute polymer solutions.

The LAOS flow of interest is a sinusoidally oscillating shear stress:

$$\Sigma(t) = \Sigma_0 \sin(2\pi\omega t) \qquad (56)$$

where ω is the dimensionless frequency of the oscillation (scaled by the polymer reptation time). This flow protocol is often referred to as LAOStress to distinguish from the more common strain-controlled protocol (LAOStrain). For the study presented here, we exclusively focus on LAOStress flows because (as we will show) it is relatively easy to construct a Lyapunov function for this protocol in the limit of large frictional couplings. The LAOStrain protocol shows similar

tendencies for SID but (as with the rate-driven steady flows) does not easily allow for comparison to an equivalent model B phase transition.

Before moving forward, we remind the reader that our calculations are a '1D' approximation of the flow, and we explicitly assume no variations in the direction of flow and vorticity. This has been established as a reasonable approximation for studying steady simple shear flow, but it is not yet known whether this approximation yields good predictions in oscillating flows. All the same, we believe that the 1D approximation is a suitable starting point for understanding certain key differences between the physics of SID in steady and unsteady flow protocols.

For the same material as before, $\theta = 120, E = 0.15, \varpi = 10^{-4}, \bar{\xi} = 0.01$ and $\bar{H} = 1$, we have performed a linear stability analysis using standard Floquet methods for oscillatory systems [40]. Briefly, we summarize the procedure by which this analysis was done. (i) First, we solved for a limit cycle (periodic) solution to a homogeneous flow for a given Σ_0 and ω. The time domain was discretized uniformly across a single period, and temporal derivatives were approximated using Fourier collocation. Limit cycle solutions were found numerically using Newton's method. (ii) With a limit cycle solution in hand, we linearized the governing equations about the limit cycle and evolved a complete set of orthogonal perturbations through a single cycle. (iii) We then performed an eigenvalue analysis of the evolved perturbations to determine whether any eigenmodes experienced a net growth through the limit cycle. (iv) Finally, we used the limit cycle obtained in (i) as an initial guess for the next deformation (incrementing Σ_0 or ω) until we covered the full range of deformation protocols of interest to the analysis.

For the material of interest ($\theta = 120, E = 0.15, \varpi = 10^{-4}, \bar{\xi} = 0.01$), the Floquet stability analysis reveals that there is a bounded unstable window in the plane of Σ_0 and ω. In Figure 12 below, the regions in grey represent conditions that are unstable to demixing.

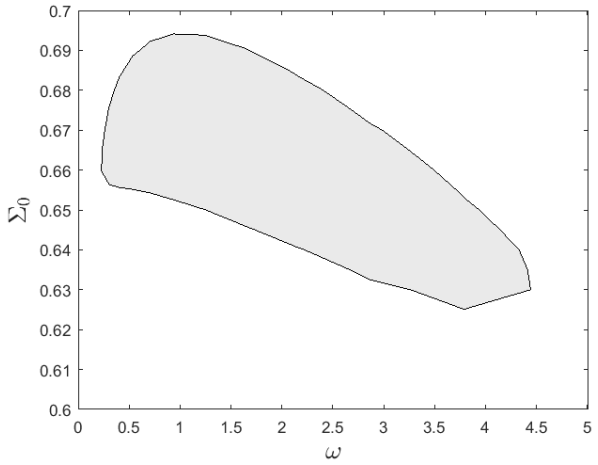

Figure 12: Linear stability boundary to SID in LAOS. The shaded region corresponds to unstable flow conditions for a system with $\theta = 120, \varpi = 10^{-4}, E = 0.15$, and $\bar{H}/\bar{\xi} \gg 1$.

As in the case of steady, simple shear there is also a second unstable window at higher Σ_0, associated with the high Wi instability window of simple shear flow [13]. For now, we will restrict our analysis to the unstable window shown above.

We can obtain a preliminary picture of the demixing instability through a full numerical simulation at one particular set of conditions. As an example, we consider a deformation with $\Sigma_0 = 0.67$ and $\omega = 0.50$. In many respects, the resulting demixing instability is remarkably similar to what has been previously observed for steady simple shear flows. Beginning from a small amount of random noise (amplitude of 10^{-5}), the system selects a preferred wavelength for the growth of inhomogeneity. Figure 13 below shows the polymer concentration profile at $t = 20$:

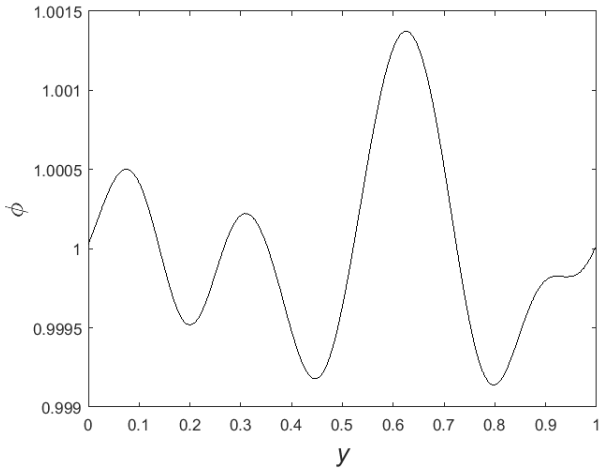

Figure 13: Snapshot of the concentration profile 20 reptation times after start-up for a system with $\Sigma_0 = 0.67, \omega = 0.5, \theta = 120, \varpi = 10^{-4}, E = 0.15, \bar{\xi} = 0.01$, and $\bar{H} = 1$. As with the case of steady simple shear flow, we find that the system selects a preferred wavelength for demixing.

As the perturbation grows, however, the system encounters a locally stable attractor characterized by a periodically oscillating inhomogeneous state. In place of a more detailed representation of the long-time limit cycle solution, we simply present snap-shots of the concentration profile at the points within the limit cycle where $L_2\phi$ is largest ($\mathrm{mod}(t, 1/2\omega) = 0.6$) and smallest ($\mathrm{mod}(t, 1/2\omega) = 0.3$). Simulations were run to $t \sim 120$, and the limit cycle shown below is clearly established by t~40.

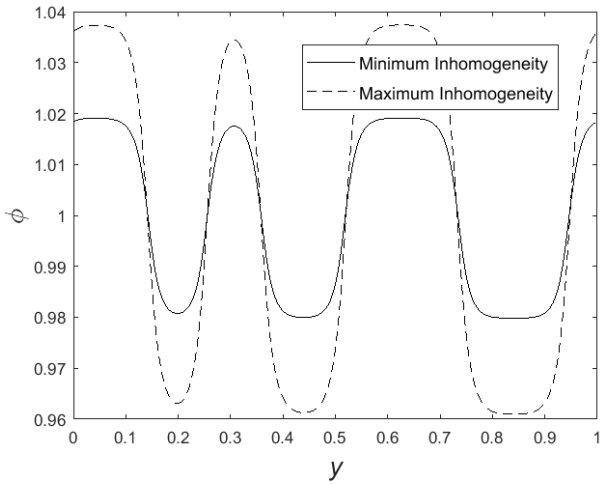

Figure 14: Snapshot of the concentration profile after more than 100 reptation times, continued from Figure 13. This oscillating concentration profile appears to be a stable attractor, and shows no signs of coarsening.

Oscillations in the amplitude of inhomogeneity are large in comparison to the mean, and there is a conspicuous lack of coarsening. Oscillations are to be expected, given that the driving force for demixing is periodic, but the lack of coarsening is more unusual; it is as though the system has become 'trapped' in the late stages of spinodal decomposition . Unlike the simple shear flow case, this result persists with increasing spatial resolution (at least up to $N = 500$) and appears to be a true solution to the governing equations rather than a numerical artifact.

We can force the system to a more coarsened state by seeding with a large perturbation that suppresses the growth of shorter wavelength modes ($\phi(0, y) = 10^{-2}\cos(2\pi y)$). However, to observe the formation of bulk shear bands (within which the concentration does not oscillate), we must also consider a much larger gap dimension. The driving force for demixing (like the imposed deformation itself) is oscillatory in nature, and so the period of oscillation encodes a characteristic diffusive lengthscale below which bulk shear bands cannot be observed. In our dimensionless units, this length-scale goes approximately as $[2\omega\overline{H}^2]^{-1/2}$, which for $\omega \sim \mathcal{O}(1)$ is much larger than the interfacial length-scale set by non-local osmotic stresses, $\bar{\xi}/\overline{H}$. Therefore, $\overline{H} \gg 1/\sqrt{2\omega}$ is required to establish bulk shear bands in the present test-case.

In the simulation below, we consider $\overline{H} = 16$. At $t = 100$, the system has nearly attained its periodic solution, and the concentration profile that emerges is somewhat unusual. Once again, we plot the system at maximum/minimum points of inhomogeneity within the (nearly) periodic solution:

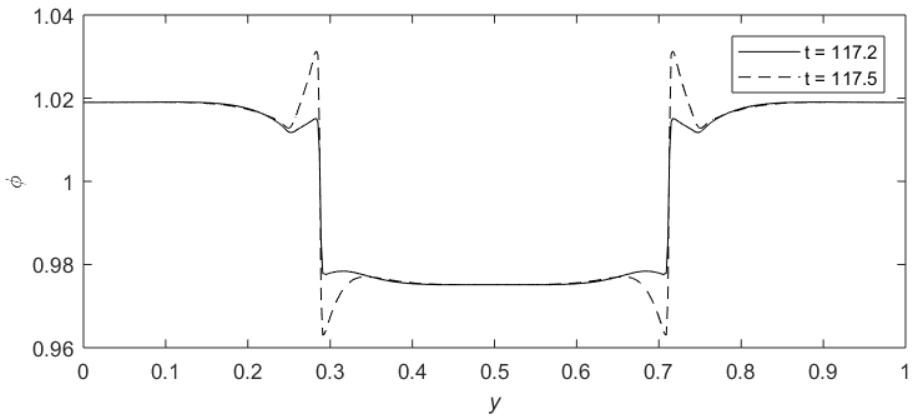

Figure 15: Snapshot of the concentration profile more than 100 reptation times after start-up. This system is sixteen times larger than the system considered in Figure 13 and Figure 14. Here, we have brought the system to a more coarsened state by initializing the system with a very large amplitude perturbation initially (comparable to half the amplitude of the fully demixed state). Here, the system appears to be converging towards a limit cycle with extended, locally homogeneous shear bands with polymer concentrations around $\phi = 0.98$ and $\phi = 1.02$.

The concentration profile in-between the two shear bands is non-monotone, which is unusual in the context of bulk demixing. Here, we find that the oscillatory driving force introduces a diffusive length-scale for the interface (dimensionless width $\left[\bar{H}\sqrt{2\omega}\right]^{-1/2}$) that in this case is much longer than the solution correlation length. If the concentration profile across the broadened interface were smooth and monotone, then a range of concentrations would be unstable to further break-up. This prevents the formation of an interface that is both smooth and broad. Instead, the otherwise broad interface develops a sharp 'crease' of width $\mathcal{O}\left(\bar{\xi}/\bar{H}\right)$, and as the 'crease' sharpens and broadens throughout the cycle, the ensuing migration-induced stresses are able to stabilize the interface to its broader overall width. With a stable interface, the system is able to establish bulk shear bands within which the concentration is not substantially changing throughout the deformation cycle.

Overall, it seems that the driving force for coarsening is suppressed when there is a conflict between the characteristic diffusive and thermodynamic length-scales for the interface. For LAOS flows that can undergo SID at higher frequencies, $\omega \gg 1/\bar{\xi}^2$, it may be that one can recover the usual coarsening dynamics, but this is beyond our scope of interest for the present report.

It may also be worth noting that Figure 14 and Figure 15 show that the mean peak-to-trough amplitude of band concentrations decreases with increasing band width. Surprisingly, this is consistent with the condition for arrested coarsening dynamics in certain models of 1D coarsening dynamics [41]

Overall, there is visual evidence that SID is initially very similar for steady and oscillatory flows (i.e. in its linear behavior), but it is evident that the non-linear aspects of SID in LAOS flows cannot be trivially extrapolated from observations of SID in steady simple shear flows. As such, wQTH does not generally hold for all LAOS flows, but it may not be immediately obvious why the two problems should look similar under some conditions (initial instability) but not others (non-linear dynamics). The simulations above offer useful insights, but it is worth pursuing a more general understanding of how and why the thermodynamic analogy breaks down in this particular case.

To pursue a proof of wQTH(a) in LAOS, we consider the same limit as before, with $\epsilon = 1/\overline{H}^2 \ll 1$. However, if one attempts to use the asymptotic model of steady simple shear flows, as defined in equations (17) - (23), then the integrated form of the total momentum balance equation is given by:

$$\Pi_{xy,0} + \varpi \frac{\partial u_{S.0}}{\partial y} = \Sigma_0 \sin\left(2\pi\omega \frac{\tau}{\epsilon}\right) \qquad (57)$$

This is clearly problematic to evaluate for $\tau > 0$ in the limit of $\epsilon \to 0$. Having asymptotically separated the stress relaxation time-scale and the mass transport time-scale, we have also asymptotically separated the mass transport timescale from the characteristic period of an oscillation. Because of this, the long-time solution must have persistent and non-trivial short time dynamics embedded. In situations like this, the leading order equations of the 'outer solution' can be solved via the method of multiple scales. We will treat the mass transport timescale τ and oscillatory timescale $t_\omega = 2\pi\omega t$ as orthogonal time-scales in the asymptotic solution. Formally, we write our asymptotic expansion as:

$$\phi(t, y, \epsilon) = \phi_0(t_\omega, \tau) + F_1(\epsilon)\phi_1(t_\omega, \tau) + \cdots \qquad (58)$$

We insert this asymptotic form of the solution into the governing equations of the full model and group all terms of equal order in ϵ. When performing these operations, one must take care in evaluating $\partial/\partial t$ derivatives because of the assumed orthogonality of t_ω and τ:

$$\frac{\partial}{\partial t}\phi_0(t_\omega, \tau) = \frac{\partial \phi_0}{\partial \tau}\left(\frac{\partial \tau}{\partial t}\right)_{t_\omega} + \frac{\partial \phi_0}{\partial t_\omega}\left(\frac{\partial t_\omega}{\partial t}\right)_{\tau} = \epsilon \frac{\partial \phi_0}{\partial \tau} + 2\pi\omega \frac{\partial \phi_0}{\partial t_\omega} \qquad (59)$$

With this change, the integrated momentum balance equation is no longer problematic:

$$\Pi_{xy,0} + \varpi \frac{\partial u_{S.0}}{\partial y} = \Sigma_0 \sin(t_\omega) \qquad (60)$$

All other momentum balance equations identically follow with the asymptotic model for steady simple shear flow. The leading order concentration equation predictably indicates no changes in concentration occurring over the oscillatory timescale:

$$\frac{\partial \phi_0}{\partial t_\omega} = 0 \qquad (61)$$

Finally, we consider the leading order solution of the constitutive equation. Migration velocities are still eliminated from the deformation terms (thereby eliminating migration induced stresses) but the viscoelasticity of the material is not lost over oscillatory timescales (i.e. time derivatives do not vanish):

$$2\pi\omega \frac{\partial Q_{ij,0}}{\partial t_\omega} + \cdots = -R_{ij}\left(Q_{ij,0}, \phi_0\right) \qquad (62)$$

Although it would seem that we have not lost the ability to apply an arbitrary initial condition (since we still have time derivatives for all variables which had time derivatives to begin with), this is not actually the case. In the method of multiple scales, we pursue solutions that are periodic in t_ω, and an arbitrary initial condition at $t_\omega = 0$ will not generally satisfy this constraint. Thus, we are still dealing with a singular asymptotic problem for which we must confirm that the behavior of the 'inner solution' at long times matches with the behavior of the outer solution at short times. This analysis follows predictably from the matching procedure in steady simple shear flow, so in the interest of concise exposition, we refer the reader to the supplementary section on the matching condition for details.

Returning to the analysis of our leading order equations of the 'outer' solution, we see that the leading order solution does not include any derivatives in τ, but does have the full set of derivatives in t_ω, and so a periodic solution in t_ω can be found. By inspection, we observe that the solution in t_ω allows a few simplifications. Most importantly, since $\phi_0$is not changing with t_ω, it must be that $\phi_0(t_\omega, \tau) = \phi_0(\tau)$. This is not surprising, since the characteristic mass transport timescale is much longer than the oscillation period in our asymptotic limit.

Next, we find that the conformation tensor and velocities vary in t_ω following a limit cycle solution to the imposed deformation given the present concentration $\phi_0(\tau)$:

$$Q_{ij,0}(t_\omega, \tau) = Q_{ij}^{LC}(t_\omega, \phi_0) \qquad (63)$$

And similarly for the polymer stress tensor:

$$\Pi_{ij,0}(t_\omega, \tau) = \Pi_{ij}^{LC}(t_\omega, \phi_0) \qquad (64)$$

Next, we seek to understand how the leading order solution changes in τ. Since the τ-dependence of the conformation tensor and velocity fields is slaved to the τ-dependence of ϕ_0, it is sufficient to learn how ϕ_0 is changing in τ. For this, we look to the $\mathcal{O}\big(F_1(\epsilon)\big) = \mathcal{O}(\epsilon)$ equation for mass transport:

$$2\pi\omega \frac{\partial \phi_1}{\partial t_\omega} + \frac{\partial \phi_0}{\partial \tau} = -\frac{\partial}{\partial y}(\phi_0 v_0) = -\frac{\partial}{\partial y}\left(\phi_0^{-\frac{1}{2}} \frac{\partial}{\partial y} \Pi_{ij,0}^{LC}(t_\omega, \phi_0)\right) \qquad (65)$$

Since τ and t_ω are orthogonal and ϕ_1 is periodic in t_ω, we can average the entire equation over a single period in t_ω to eliminate all explicit t_ω dependencies:

$$\frac{\partial \phi_0}{\partial \tau} = -\frac{\partial}{\partial y}\left(\phi_0^{-1/2} \frac{\partial}{\partial y} \langle \Pi_{ij,0}^{LC}(\phi_0) \rangle\right) \qquad (66)$$

$$\langle \Pi_{ij,0}^{LC}(\phi_0) \rangle = \int_0^1 \Pi_{ij,0}^{LC}(t_\omega, \phi_0) \qquad (67)$$

From this point, it is trivial to reconstruct the mapping to model B following the procedure outlined in equations (27)-(41). We also point out that a first correction to the polymer concentration profile predicts periodic oscillations at the interface as the system moves through portions of the limit cycle that favor mixing/demixing.

$$\frac{\partial \phi_1}{\partial t_\omega} = -\frac{\partial}{\partial y}\left(\phi_0^{-1/2}\frac{\partial}{\partial y}\left[\Pi_{ij,0}^{LC}(t_\omega, \phi_0) - \langle \Pi_{ij,0}^{LC}(\phi_0)\rangle\right]\right) \qquad (68)$$

This oscillatory behavior of the interface is a small correction to the leading order dynamics in the high coupling friction limit, but it becomes an $\mathcal{O}(1)$ effect at the interface when the coupling friction is set to a lower, more realistic value (as demonstrated by the earlier numerical simulation).

Looking towards a proof of wQTH(b) under LAOS flows, we first consider whether the existence and location of the SID instability are identical for the asymptotic model and the full model. Following the same series of arguments posed for the simple shear case, one can show that the boundaries of the unstable window will always match the asymptotic model predictions when the system is macroscopic and the coupling friction is assigned a realistic value. This result has been confirmed numerically as well.

Next, we consider whether the non-linear predictions of the asymptotic model are in agreement with the predictions of the full model. For the simple shear flow case, there was good agreement; steady state predictions only differed by negligible $\mathcal{O}(\varpi)$ solvent effects. In the oscillatory flow case, however, the dynamics at the interface between shear bands can differ by $\mathcal{O}(1)$ effects from the 'breathing' modes. These disparities at the interface are actually very important: in any demixing event that allows the formation of bulk regions, the interfacial stresses are responsible for driving coarsening and selecting the composition in the limiting bulk regions.

Finally, we confirm that the asymptotic model predictions for bulk shear band concentrations, ϕ^I, ϕ^{II} are substantially different from what is observed in the full model

calculations. In Figure 18 below, for example, we plot the predicted limiting concentrations as dotted lines, superimposed over the concentration profiles observed around $t = 117$, as described in Figure 15. At this time, the system has not yet converged to a perfectly periodic solution, but it is close enough that the existence of a stable attractor is evident and the quantitative differences in the two predictions are representative. Despite the quantitative disparity, it is worth noting that the oscillations at the interface do not disallow the *existence* of bulk shear banded steady states, as predicted by the asymptotic model.

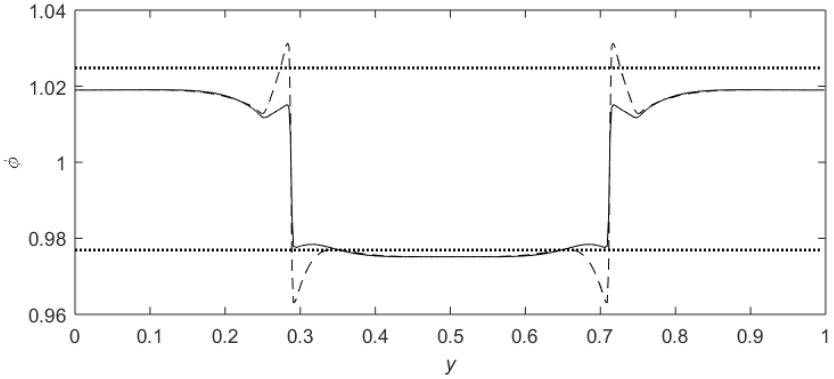

Figure 16: Superimposing the predicted shear band concentrations (dashed lines) from the asymptotic model on the observed concentration profile from the full model. Note that the disparity between the two predictions is now much larger than $\mathcal{O}(\varpi)$, owing to the $\mathcal{O}(1)$ effects of migration-induced stresses acting at the interface.

Overall, we find that our asymptotic model provides an insightful description of the leading order physics relevant to LAOS SID in our two-fluid model, especially as pertains to the boundaries of the unstable window. In the limited context, we may regard wQTH as true for LAOS flows. More generally, however, thermodynamic intuitions do not predict non-linear aspects of SID instabilities in LAOS.

Finally, we recognize that the study of LAOS induced demixing we present here has been necessarily limited in scope, and there are a number of very interesting directions for future work

on this subject. With respect to future studies that focus on two-fluid model predictions, we suggest that the most profitable topics for future research will be (1) 2D and 3D resolution of the demixing instability, and (2) a more detailed understanding of the mechanism by which fluctuations of an interface create viscoelastic stresses. The former question will be relevant for comparison to experimental studies of SID in LAOS, while the latter could have broader applications for viscoelastic phase separation phenomena (e.g. the 'moving droplet phase' observed in quiescent phase separations [22]).

8. Summary and Conclusions

We have studied the non-linear dynamics of shear induced demixing instabilities as modelled by a two-fluid model of a semi-dilute entangled polymer solution in 1D simple shear flow. Reviewing the existing literature on the subject, we describe a sort of paradox: shear induced demixing instabilities are not thermodynamically driven, but for practical purposes they can behave as though they were.

To resolve this paradox, we derive an asymptotic limit of the two-fluid model that preserves the essential character of the instability while simplifying the governing equations to the point where a Liapunov functional $\mathcal{L}$ can be determined. This Liapunov functional is a non-equilibrium analogue to the free energy, in the sense that the dynamics of the system can be interpreted in terms of a tendency to minimize the value of $\mathcal{L}$.

Using the Liapunov functional, we explore questions pertaining to the onset of SID instabilities, the selection of an inhomogeneous steady state, and the intermediate dynamics in-between. We also consider predictions of finite amplitude instabilities in homogeneous shear

flow. In each case, the predictions of the asymptotic model are qualitatively consistent with numerical simulations of the full model.

Finally, we have presented two counter-examples where thermodynamic intuitions of SID are apparently not correct. In the first example, we consider simple shear flows driven by a constant boundary velocity (as opposed to a constant shear stress). In this case, the exchange of constraints cannot be handled via the usual method of Legendre transforms because shear stress and shear rate are not conjugate variables in inhomogeneous shear flow. In the second example, we consider simple shear flows driven by an unsteady (oscillatory) boundary shear stress. Here, the time-dependence of the deformation protocol introduced a diffusive length-scale to compete with the natural thermodynamic length-scale at which an interface is expected to form. As a result, we observed a conspicuous lack of coarsening following the initial demixing instability.

Overall, we believe that the present work offers a well-reasoned and relatively complete consideration of SID (and its relation to thermodynamic instabilities) as modelled by a two-fluid model of semi-dilute entangled polymer solutions in '1D' simple shear flow. This work is an essential pre-requisite for future studies that explore the character of SID instabilities in 2D and 3D, as is needed for a complete comparison to experiments.

Acknowledgements

This work was primarily supported by the Fluid Mechanics program under NSF grant CBET-1510333, and also by the CMMT Program under grant DMR-1822215.

Appendix

A.1 Matching procedure for Asymptotic Model

Here, we present the details of matching the 'inner solution' and 'outer solution' for the dynamics of SID under asymptotically large coupling friction ($\epsilon = 1/\bar{H}^2 \ll 1$ for fixed $\bar{\xi}/\bar{H}$). For the inner solution, we seek an asymptotic solution of the form:

$$\phi(t, y, \epsilon) = f^0(\epsilon)\phi^0(t, y) + f^1(\epsilon)\phi^1(t, y) + \cdots$$

And likewise for all other dynamical variables in the problem. Note that we distinguish the inner solution from the outer solution by the use of superscripts instead of subscripts. As was true for the outer solution, we know that $f^0(\epsilon) = 1$ because the polymer concentration is not vanishing in the limit of $\epsilon \to 0$. Therefore, the leading order equations of the inner solution are given by:

$$\frac{\partial \phi^0}{\partial t} = 0 \qquad (69)$$

$$\Sigma_0 = \Pi^0_{xy} + E\varpi \frac{\partial u^0_S}{\partial y} \qquad (70)$$

$$u^0_P - u^0_S = 0 \qquad (71)$$

$$v^0_P = (\phi^0)^{-3/2} \frac{\partial \Pi^0_{yy}}{\partial y} \qquad (72)$$

$$\frac{\partial Q^0_{xx}}{\partial t} - 2Q^0_{xy} \frac{\partial u^0_P}{\partial y} = -R^0_{xx} \qquad (73)$$

$$\frac{\partial Q^0_{yy}}{\partial t} = -R^0_{yy} \qquad (74)$$

$$\frac{\partial Q_{zz}^0}{\partial t} = -R_{zz}^0 \qquad (75)$$

$$\frac{\partial Q_{xy}^0}{\partial t} - Q_{yy}^0 \frac{\partial u_P^0}{\partial y} = -R_{xy}^0 \qquad (76)$$

The inner solution retains a full complement of time derivatives, so one can determine how the system evolves from an arbitrary initial condition. Considering the polymer concentration, ϕ^0, we see that the initial condition is frozen in for all t. The polymer conformation tensor, on the other hand, undergoes a complex series of viscoelastic transients before it eventually converges towards the steady state solution for the frozen-in concentration profile. Fortunately, for any reasonable choice of initial conditions in the conformation tensor, the system always tends toward the same steady state solution, $\boldsymbol{Q}^{SS}(\phi^0, \Sigma_0)$:

$$\lim_{t\to\infty}[\boldsymbol{Q}^0(\boldsymbol{Q}^0(t=0), \phi^0, t, \Sigma_0)] = \boldsymbol{Q}^{SS}(\phi^0, \Sigma_0) \qquad (77)$$

Next, we return to a consideration of the outer solution to the problem, where time is rescaled to $\tau = \epsilon t$ and the asymptotic solution has the form:

$$\phi(\tau, y, \epsilon) = F_0(\epsilon)\phi_0(\tau, y) + F_1(\epsilon)\phi_1(\tau, y) + \cdots \qquad (78)$$

As before, we recognize that $F_0(\epsilon) = 1$ because the fraction of polymer in the system is not vanishing as $\epsilon \to 0$. Once again, the leading order equations for the outer solution are given by:

$$\frac{\partial \phi_0}{\partial \tau} = \frac{\partial}{\partial y}\left(\phi_0 v_{P,0}\right) \qquad (79)$$

$$\Sigma_0 = \Pi_{xy,0} + E\varpi \frac{\partial u_{S,0}}{\partial y} \qquad (80)$$

$$u_{P,0} = u_{S,0} \qquad (81)$$

$$v_{P,0} = \phi_0^{-3/2} \frac{\partial \Pi_{yy,0}}{\partial y} \qquad (82)$$

$$2Q_{xy,0} \frac{\partial u_{P,0}}{\partial y} = R_{xx,0} \qquad (83)$$

$$0 = R_{yy,0} = R_{zz,0} \qquad (84)$$

$$Q_{yy,0} \frac{\partial u_{P,0}}{\partial y} = R_{xy,0} \qquad (85)$$

At $\tau = 0$, the initial condition of the outer solution must match with the long time behavior of the inner solution. Formally, we write:

$$\lim_{t \gg 1} \left[\phi^0(t,y) + \mathcal{O}\left(f^1(\epsilon)\right)\right] \Leftrightarrow \lim_{\tau \ll 1} \left[\phi_0(\tau,y) + \mathcal{O}\left(F_1(\epsilon)\right)\right] \qquad \text{as } \epsilon \to 0$$

And likewise for all other time-dependent variables.

At time $\tau = 0$, the initial condition for ϕ_0 in the outer solution must be identical to the initial condition for ϕ^0 in the inner solution, since $\lim_{t \gg 1} \phi^0(t,y) = \phi^0(0,y)$.

Considering the conformation tensor, we once again see the importance of the matching procedure. The conformation tensor is set by the polymer concentration and applied shear stress, $\boldsymbol{Q}_0 = \boldsymbol{Q}_0(\phi_0, \Sigma_0)$, but when such a solution is not unique (i.e. multiple stationary solutions exist) it is not a-priori obvious which branch of solutions applies to the dynamics of the problem. The matching condition resolves this conundrum, specifying the physically meaningful branch of

solutions as the branch which matches the long-time dynamics that follow after a start-up with fixed concentration:

$$\boldsymbol{Q}_0(\phi_0, \Sigma_0) = \lim_{t\to\infty}[\boldsymbol{Q}^0(\boldsymbol{Q}^0(t=0), \phi_0, t, \Sigma_0)] = \boldsymbol{Q}^{SS}(\phi_0, \Sigma_0)$$

This matching procedure establishes agreement between the inner and outer solution at $t \to \infty$ and $\tau = 0$, but we must also determine how the mismatch vanishes for $t \gg 1$ and $\tau \ll 1$ when $\epsilon \to 0$. For this, we note that a smooth initial condition in ϕ_0 gives dynamics that are smooth at $\tau = 0$. In other words, provided ϕ_0 is smooth, time derivatives of all orders are computable at every point in space at $\tau = 0$:

$$\frac{\partial \phi_0}{\partial \tau} = \frac{\partial}{\partial y}\left[M(\phi_0)\frac{\partial}{\partial y}\left[\frac{\delta \mathcal{L}}{\delta \phi}\right]\right]$$

$$\frac{\partial^2 \phi_0}{\partial \tau^2} = \frac{\partial}{\partial y}\left[\left(\frac{\partial M}{\partial \phi_0}\frac{\partial \phi_0}{\partial \tau}\right)\frac{\partial}{\partial y}\left[\frac{\delta \mathcal{L}}{\delta \phi}\right] + \cdots\right]$$

And so on. Since all other variables are slaved to the concentration, those dynamics are likewise smooth, provided the underlying constitutive behavior is also smooth and monotonic (invertible). For example, the time derivatives at $\tau = 0$ for the conformation tensor can be computed by:

$$\frac{\partial \boldsymbol{Q}_0}{\partial \tau} = \left(\frac{\partial \boldsymbol{Q}_0^{SS}}{\partial \phi_0}\right)_{\Sigma_0}\frac{\partial \phi_0}{\partial \tau}$$

$$\frac{\partial^2 \boldsymbol{Q}_0}{\partial \tau^2} = \left(\frac{\partial \boldsymbol{Q}_0^{SS}}{\partial \phi_0}\right)_{\Sigma_0}\frac{\partial^2 \phi_0}{\partial \tau^2} + \left(\frac{\partial^2 \boldsymbol{Q}_0^{SS}}{\partial \phi_0^2}\right)_{\Sigma_0}\left(\frac{\partial \phi_0}{\partial \tau}\right)^2$$

And so on. Thus, for all dynamical variables in the outer solution, we can say that in the limit of $\tau \to 0$, any change occurring within the system must be linear in τ to leading order. For example, in the concentration profile, we must have:

$$\lim_{\tau \ll 1}\big(\phi_0(\tau, y)\big) = \phi_0(0, y) + \tau\left(\frac{\partial \phi_0}{\partial \tau}\right)_{\tau=0} + \mathcal{O}(\tau^2)$$

And likewise for all other dynamical variables in the problem. Returning to the matching condition, we then find that the mismatch is $\mathcal{O}(\epsilon)$, since $\tau = \epsilon t$:

$$\lim_{t \gg 1}\left[\phi^0(0, y) + \mathcal{O}\big(f^1(\epsilon)\big)\right] \Leftrightarrow \lim_{\tau \ll 1}\left[\phi_0(0, y) + \tau\left(\frac{\partial \phi_0}{\partial \tau}\right)_{\tau=0} + \mathcal{O}(\tau^2)\right] \qquad \text{as } \epsilon \to 0$$

$$\lim_{t \gg 1}\left[\mathcal{O}\big(f^1(\epsilon)\big)\right] \Leftrightarrow \lim_{\tau \ll 1}\left[\tau\left(\frac{\partial \phi_0}{\partial \tau}\right)_{\tau=0} + \mathcal{O}(\tau^2)\right] \qquad \text{as } \epsilon \to 0$$

$$f^1(\epsilon) = \epsilon$$

From this point, one can proceed to compute higher order corrections to the inner/outer solutions. For steady simple shear flows, the leading order equations of the inner and outer solutions are useful and informative, so higher order corrections are less important. However, this will not always be the case: for complex 2D/3D flows in macroscopic geometries, it is not always easy (or interesting) to evaluate an outer solution. However, if one can obtain a leading order inner solution and its first correction, this can provide insights for understanding the effects of stress/concentration coupling and stress-induced migration.

3.2. Lees Edwards Boundary Conditions

Solving these equations for a macroscopic system is computationally prohibitive due to both spatial and temporal stiffness concerns ($\bar{\xi}/\bar{H} \sim 10^{-5}$). In such cases is often better to simulate a basis set of representative 'small' systems, from which one can extrapolate the behavior of a macroscopic system. For studies of model B phase separations, periodic boundary conditions are a preferred means of selecting smaller systems for two reasons: first, for studying bulk demixing behavior periodic boundary conditions eliminate any influence of solid walls, and second, periodic boundary conditions permit the use of very efficient computational strategies (e.g. fast Fourier transforms for spatial differentiation).

Therefore, for the purposes of this report, we will use Lees-Edwards boundary conditions; all variables except u_P and u_S are assumed to be periodic, while u_P and u_S have a 'jump' discontinuity across the boundary [28], since the imposed deformation requires a net increase in the flow velocity from $y = 0$ to $y = 1$. In practice, we eliminate the jump discontinuity by solving for $\dot{\gamma}_S = \partial_y u_S$ and $\dot{\gamma}_P = \partial_y u_P$, replacing equation (3) with its spatial derivative:

$$\dot{\gamma}_P - \dot{\gamma}_S = \frac{1}{\bar{H}^2}\frac{\partial}{\partial y}\left[\phi^{-\frac{3}{2}}\frac{\partial \Pi_{xy}}{\partial y}\right] \qquad (86)$$

Periodic boundary condition are then assigned for all variables:

$$\phi(y=0) = \phi(y=1) \qquad Q(y=0) = Q(y=1) \qquad (87)$$

$$\dot{\gamma}_P(y=0) = \dot{\gamma}_P(y=1) \qquad \dot{\gamma}_S(y=0) = \dot{\gamma}_S(y=1) \qquad (88)$$

A.2 Brief review of 1D phase transitions in model B

In the main body of this work, we have shown that there are important mathematical similarities between the linear and non-linear dynamics of SID and the simplest class of continuum phase separations in a non-flowing system: model B of the Halperin-Honenberg classification scheme [25]. Model B describes phase separations through purely diffusive transport down chemical potential gradients. Here, we employ a 1D version of model B so that variations in composition are constrained to occur only in one direction (as is approximately seen in 2D simulations of SID [11]).

For model B in 1D, the tranpport equation for a species with volume fraction ϕ is given by :

$$\frac{\partial}{\partial t}\phi = \frac{\partial}{\partial y}\left[M(\phi)\frac{\partial}{\partial y}\left[\frac{\delta F}{\delta \phi}\right]\right] \qquad (89)$$

where $M > 0$ is the species mobility, F is the system free energy, and t, y are temporal and spatial coordinates. The free energy typically entails both a local (bulk) free energy of mixing f_L and a non-local (interfacial) free energy f_{NL} due to gradients in concentration:

$$F = \int dy[f_L(\phi) + f_{NL}(\phi, \nabla\phi)] \qquad (90)$$

A simple functional form for $f_{NL}(\phi, \nabla\phi)$ is [42]:

$$f_{NL} = \frac{1}{2}\Gamma(\phi)|\nabla\phi|^2 \qquad (91)$$

where $\Gamma(\phi)$ is related to the free energy of forming an interface (e.g. abrupt change in concentration). Assuming a rigid wall on either side of the system, we use boundary conditions that ensure no-flux:

$$\frac{\partial}{\partial y}\frac{\delta F}{\delta \phi} = 0 \qquad (92)$$

We further assume that the rigid wall is a neutrally interacting surface (i.e. chemically reflecting) so that gradients in concentration vanish at the boundary:

$$\frac{\partial \phi}{\partial y} = 0 \qquad (93)$$

We can confirm that deterministic trajectories of ϕ never increase the system free energy at any time, and the model is therefore thermodynamically consistent:

$$\frac{\partial F}{\partial t} = \int dy \left[\frac{\delta F}{\delta \phi}\frac{\partial \phi}{\partial t}\right] = -\int dy \left[M(\phi)\left(\frac{\partial}{\partial y}\left[\frac{\delta F}{\delta \phi}\right]\right)^2\right] \leq 0 \qquad (94)$$

In the general language of non-linear dynamics, we have confirmed that the free energy is a Lyapunov functional for the dynamics (to within an added constant). This property of the free energy ensures that thermodynamic intuitions about stable and metastable states will be rightly reflected in the model's dynamics (i.e. the system evolves to minimize its free energy, and the lowest free energy state is always most stable).

It is a short but worthwhile exercise to reproduce the 1D linear stability analysis of model B. Supposing a homogeneous base state, $\phi = \phi_o$, we apply an infinitesimal perturbation, $\phi = \phi_o + \delta\phi$. The transport equation for $\delta\phi$ then becomes:

$$\partial_t \delta\phi = M(\phi_o)\frac{\partial^2}{\partial y^2}\left[\delta\phi\left(\frac{\partial^2 f_L}{\partial \phi^2}\right)_{\phi=\phi_o} - \Gamma(\phi_o)\frac{\partial^2}{\partial y^2}\delta\phi\right] \qquad (95)$$

This is a linear PDE equation with solutions of the form $\delta\phi \sim e^{\sigma t}\cos(ky)$, with growth rate σ and wave-number $k = n\pi/H$ for $n = 1, 2, 3, \ldots$ and system size H. Inserting this functional form for $\delta\phi$ into equation (95), we obtain a dispersion relationship for the growth rate σ in terms of the wave-number, k:

$$\sigma = -M(\phi_o)k^2\left[\left(\frac{\partial^2 f_L}{\partial\phi^2}\right)_{\phi=\phi_o} + \Gamma(\phi_o)k^2\right] \qquad (96)$$

The system is linearly unstable to demixing when $\sigma > 0$, which implies:

$$\left(\frac{\partial^2 f_L}{\partial\phi^2}\right)_{\phi=\phi_o} + \Gamma(\phi_o)\left(\frac{\pi}{H}\right)^2 < 0 \qquad (97)$$

The first term represents the condition for bulk thermodynamic instability, and the second term is a correction for confinement over a finite system size H. Note that it is the longest wavelength ($k = \pi/H$) that determines the stability boundary. When a demixing instability occurs, there is a preferred wavelength, λ_M, over which variations in concentration are most likely to emerge. This wavelength can be derived from $\sigma/\partial k = 0$:

$$\lambda_M = 2\pi\left[-\frac{1}{2\Gamma(\phi_o)}\left(\frac{\partial^2 f_L}{\partial\phi^2}\right)_{\phi=\phi_o}\right]^{-1/2} \qquad (98)$$

In the context of model B, the exponential growth in amplitude of inhomogeneity with a preferred wavelength is called 'spinodal decomposition', and the boundaries within which this instability develops are called the 'spinodal lines'. In the terminal stages of spinodal decomposition, the perturbation amplitude saturates to a banded structure (in 1D) with extended,

locally homogeneous regions alternating between a high and low concentration state. Over much longer time-scales, these bands ripen together, decreasing the total number of bands and increasing the average size of a band. The average domain size grows logarithmically in time, and the process does not terminate until the system reaches the minimum number of bands that can be realized in the system under consideration (two for macroscopic phase separation or three for periodic boundary conditions) [23] [24]. Arrested coarsening is not possible in this system; any compositionally inhomogeneous state possessing more than the minimum number of bands is linearly unstable.

Throughout the coarsening process, the compositions of the extended locally homogeneous regions asymptotically approach the compositions of the bulk phases that coexist at equilibrium. These compositions, ϕ^I and ϕ^{II}, can be found by minimizing the free energy of the system, often graphically represented by a 'common tangent' line across a double-welled potential f_L [15], as illustrated in the cartoon below:

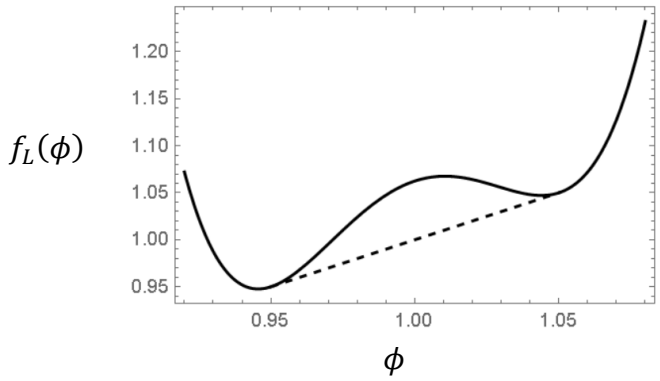

Figure 17: Graphical representation of the common tangent rule that encodes the selection of a phase separated steady state following a demixing instability in model B. In this case, a homogeneous material ($\phi = 1$) will demix into phases with $\phi^I = 0.95$ and $\phi^{II} = 1.05$, as indicated by the intersection of the common tangent (dashed curve) with the homogeneous potential landscape (solid curve). The common tangent rule can be constructed from arguments of free energy minimization or from the equality of osmotic pressures and chemical potentials between the two phases.

Equivalently, ϕ^I and ϕ^{II} can be found by balancing the bulk osmotic pressure $\pi_L(\phi) = \phi\mu_L(\phi) - f_L(\phi)$ and the chemical potential $\mu_L(\phi) = \partial f_L/\partial\phi$ within the two phases:

$$\mu_L(\phi^I) = \mu_L(\phi^{II}) \qquad \pi_L(\phi^I) = \pi_L(\phi^{II}) \qquad (99)$$

The set of compositions ϕ^I and ϕ^{II} that may co-exist at equilibrium form the 'binodal' lines. For a range in temperature (or pressure) and composition, the spinodal and binodal lines comprise an equilibrium phase diagram [15]. Any bulk system whose mean concentration lies between the spinodal lines is linearly unstable to fluctuations when homogeneous, and stable only when it is macroscopically phase separated. By contrast, any bulk system whose mean concentration lies between the binodal and spinodal lines is linearly stable for both homogeneous and macroscopically phase separated states. However, the free energy of the phase separated state of such a system is always lower, so homogeneous states between the spinodal and binodal lines are metastable and subject to demixing along a pathway of nucleation and growth [15] [43]. As such, linear stability analysis alone will under-estimate a system's susceptibility to phase separation under normal experimental conditions.

A.3 Table of variables

Variable	Definition
t	Time, scaled by the equilibrium reptation time, $\tau_D(\phi_o)$
τ	Time, scaled by the diffusion time, $\tau_D(\phi_o)/\bar{H}^2$
t_ω	Time, scaled by the period of an oscillation, $\tau_D(\phi_o)/\omega$
x	Spatial position in the flow direction (not used in the '1D' approximation)
y	Spatial position in the flow gradient direction, scaled by gap size H
z	Spatial position in the vorticity direction (not used in '1D' approximation)
ϕ	Polymer volume fraction, scaled by equilibrium mean value ϕ_o
$\boldsymbol{u}_X$	Velocity vector of component X
u_X	Velocity in the flow direction (x) for component X
v_X	Velocity in the flow gradient (y) direction for component X, scaled by H/τ_D

Q_{ij}	ij-component of polymer Conformation tensor, $\boldsymbol{Q}$
Π_{ij}	ij-component of polymer stress tensor $\boldsymbol{\Pi}$ (elastic and osmotic combined)
π_{ij}	ij-component of an osmotic pressure tensor $\boldsymbol{\pi}$
μ	Denotes a chemical potential (or an 'effective' analogue)
R_{ij}	ij-component of a stress relaxation tensor $\boldsymbol{R}$
X_0	Denotes the leading order 'outer' solution (long times) for variable X
X^0	Denotes the leading order 'inner' solution (short times) for variable X
ϵ	Small parameter, $1/\bar{H}^2$, for the high coupling friction limit
E	Ratio of elastic modulus, $G(\phi_o)$ to osmotic modulus, $\chi_0^{-1}\phi_o^2$
θ	Ration of reptation time to longest Rouse reorientation time
Z	Average number of tube segments per chain
$\bar{\xi}$	Ratio of solution correlation length, ξ, to gap dimension H
$\bar{H}$	Ratio of gap dimension H to magic length ℓ_C
ϖ	Ratio of solvent viscosity to polymer zero shear viscosity
Wi	Dimensionless overall shear rate, scaled by $1/\tau_D(\phi_o)$
Σ_0	Dimensionless shear stress, scaled by shear modulus $G(\phi_o)$
ω	Dimensionless period of an oscillation, scaled by the reptation time $\tau_D(\phi_o)$
ϕ_o	Mean volume fraction of polymer at equilibrium
$G(\phi_o)$	Shear modulus of polymer solution at volume fraction ϕ_o
$\tau_D(\phi_o)$	Reptation time of the polymer
τ_R	Longest Rouse reorientation time of the polymer
ℓ_C	Length where stress relaxation and diffusion occur at same time, $\ell_C^2 = D_{eq}\tau_D(\phi_o)$
D_{eq}	Equilibrium diffusion coefficient for long wavelength perturbations
$\zeta(\phi_o)$	Drag coefficient for polymer and solvent at equilibrium
χ_0^{-1}	Osmotic susceptibility of the polymer solution at equilibrium
M	Mobility
F	Free energy
$\mathcal{L}$	Lyapunov functional
$f_L(\phi)$	Local (bulk) free energy density of mixing
f_{NL}	Non-local free energy density of mixing (related to concentration gradients)
Λ	A contribution to $\mathcal{L}$ arising from elastic forces induced by flow
f_Λ	'effective' free energy density from local contributions to $\mathcal{L}$
δX	Denotes a linear perturbation on parameter X (except when it is a functional deriv)
σ	Growth rate for a perturbation
k	Wavenumber for a perturbation
X^I, X^{II}	Values of variable X in coexisting phases states I and II after demixing.
y^I, y^{II}	Denotes the volume fraction of the system in states I and II after demixing
$\dot{\gamma}_X$	Local shear rate $\partial u_X/\partial y$ of fluid X
N	Number of grid points used in a numerical simulation
$L_2\phi$	$L2$ norm for departure from homogeneity in the concentration profile
$L_2\nabla\phi$	$L2$ norm for departure from homogeneity in the concentration gradient

References

[1] C. Rangel-Nafaile, A. B. Metzner and K. F. Wissbrun, "Analysis of stress-induced phase separations in polymer solutions," *Macromolecules,* vol. 17, pp. 1187-1195, 1984.

[2] E. Helfand and G. Fredrickson, "Large Fluctuations in Polymer Solutions Under Shear," *Physical Review Letters,* vol. 62, no. 21, pp. 2468-2471, 1989.

[3] A. Onuki, "Shear-Induced Phase Separations in Polymer Solutions," *Journal of the Physical Society of Japan,* vol. 59, no. 10, pp. 3427-3430, 1990.

[4] S. T. Milner, "Dynamical theory of concentration fluctuations in polymers under shear," *Physical Review E,* vol. 48, no. 5, pp. 3674-3691, 1992.

[5] M. Doi and A. Onuki, "Dynamic coupling between stress and composition in polymer solutions and blends," *J. Phys. II France,* vol. 2, no. (8), pp. 1631-1656, 1992.

[6] H. Ji and E. Helfand, "Concentration Fluctuations in Sheared Polymer Solutions," *Macromolecules,* vol. 28, pp. 3869-3880, 1995.

[7] S. M. Fielding and P. D. Olmstead, "Flow phase diagrams for concentration-coupled shear banding," *Euro. Phys. J. E,* vol. 11, pp. 65-83, 2003.

[8] S. M. Fielding and P. D. Olmstead, "Kinetics of the shear banding instability in startup flows," *Physical Review E,* vol. 68, no. 3, 2008.

[9] M. Cromer, M. Villet, G. Fredrickson and L. G. Leal, "Shear banding in polymer solutions," *Physics of Fluids,* vol. 25, p. 051703, 2013.

[10] M. Cromer, G. Fredrickson and L. G. Leal, "A study of shear banding in polymer solutions," *Physics of Fluids,* vol. 26, p. 063101, 2014.

[11] L. Jupp, T. Kawakatsu and X.-F. Yuan, "Modeling shear-induced phase transitions of binary polymer mixtures," *Journal of Chemical Physics,* vol. 119, no. 12, pp. 6361-6372, 2003.

[12] L. Jupp and X.-F. Yuan, "Dynamic phase separation of a binary polymer liquid with asymmetric composition under rheometric flow," *J. Non-Newtonian Fluid Mech.,* vol. 124, pp. 93-101, 2004.

[13] J. D. Peterson, M. Cromer, G. H. Fredrickson and L. G. Leal, "Shear banding predictions for the two-fluid Rolie-Poly model," *Journal of Rheology,* vol. 60, pp. 927 - 951, 2016.

[14] S. T. Milner, "Effects of Shear Flow on Semi-Dilute Polymer Solutions," *Theoretical Challenges in the Dynamics of Complex Fluids (T.C.B. McLeish ed.), Kluwer Acad. Pub (Netherlands),* pp. 127-140, 1997.

[15] A. Novick-Cohen and L. A. Segel, "Nonlinear Aspects of the Cahn-Hilliard Equation," *Physica 10D,* pp. 277-289, 1983.

[16] K. Migler, C.-H. Liu and D. J. Pine, "Structure Evolution of a Polymer Solution at High Shear Rates," *Macromolecules,* vol. 29, pp. 1422-1432, 1995.

[17] P. G. de Gennes, Scaling Concepts in Polymer Physics, Ithaca: Cornell Univ. Press, 1979.

[18] M. Cromer, M. C. Villet, G. H. Fredrickson, L. G. Leal, R. Sepanyan and M. J. Bulters, "Concentration fluctuations in polymer solutions under extensional flow," *Journal of Rheology,* vol. 57, pp. 1211-1235, 2013.

[19] T. Hashimoto and T. Kume, ""Butterfly" Light Scatting Pattern Formed in Shear-Enhanced Concentration Fluctuations in Polymer Solutions and Anomaly at High Shear Rates," *Journal of the Physical Society of Japan,* vol. 61, no. 6, pp. 1839-1843, 1992.

[20] X.-L. Wu, D. J. Pine and P. K. Dixon, "Enhanced Concentration Fluctuations in Polymer Solutions in Shear Flow," *Physical Review Letters,* vol. 66, no. 18, pp. 2408-2411, 1991.

[21] N. Clarke and T. C. B. McLeish, "Shear flow effects on phase separation of entangled polymer blends," *Physical Review Letters E,* vol. 57, no. 4, pp. 3731-3734, 1998.

[22] H. Tanaka, "Viscoelastic phase separation," *J. Phys.: Condens. Matter,* vol. 12, pp. 207-264, 2000.

[23] J. S. Langer, "Theory of Spinodal Decomposition in Alloys," *Annals of Physics,* vol. 65, pp. 53 - 86, 1971.

[24] K. Kawasaki and T. Ohta, "Kink dynamics in one-dimensional nonlinear systems," *Physica,* vol. 116A, pp. 573-593, 1982.

[25] P. C. Honenberg and B. I. Halperin, "Theory of Dynamic Critical Phenomena," *Rev. Mod. Phys.,* vol. 49, p. 435, 1977.

[26] A. E. Likhtman and R. S. Graham, "Simple constitutive equation for linear polymer melts derived from molecular theory: Rolie-Poly equation," *J. Non-newtonian Fluid Mech.,* vol. 114, pp. 1-12, 2003.

[27] R. S. Graham, A. E. Likhtman, T. C. B. McLeish and S. T. Milner, "Microscopic theory of linear, entangled polymer chains under rapid deformation including chain stretch and convective constraint release," *Journal of Rheology,* vol. 47, p. 1171, 2003.

[28] A. Onuki, R. Yamamoto and T. Taniguchi, "Phase Separation in Polymer Solutions Induced by Shear," *J. Phys. II France,* vol. 7, pp. 295-304, 1997.

[29] P. A. Vasquez, L. P. Cook and G. McKinley, "A network scission model for wormlike micellar solutions I: Model formulation and homogeneous flow predictions," *Journal of Non-Newtonian Fluid Mechanics,* vol. 144, no. 2, pp. 122-139, 2007.

[30] V. G. Mavrantzas and A. N. Beris, "Modeling of the rheology and flow-induced concentration changes in polymer solutions," *Phys. Rev. Lett. ,* vol. 70, p. 2659, 1993.

[31] A. N. Beris and V. G. Mavrantzas, "On the compatibility between various macroscopic formalisms for the concentration and flow of dilute polymer solutions," *Journal of Rheology,* vol. 38, pp. 1235-1250, 1994.

[32] H. Khalil, Nonlinear Systems, Upper Saddle River, NJ: Prentice Hall, 1996.

[33] P. J. Flory, "Thermodynamic Relations for High Elastic Materials," *Transactions of the Faraday Society,* vol. 57, p. 829, 1961.

[34] V. Schmitt, C. M. Marques and F. Lequeux, "Shear-Induced Phase Separation of Complex Fluids-The Role of Flow-Concentration Coupling," *Physical Review E,* vol. 52, pp. 4009-4015, 1995.

[35] D. Jou, J. Casas-Vasquez and M. Criado-Sancho, Thermodynamics of Fluids under Flow, New York: Springer, 2011.

[36] P. Nozieres and D. Quemada, "A Possible Instability Mechanism for Plug Formation in a Sheared Suspension Flow," *Europhysics Letters,* vol. 2, no. 2, pp. 129-135, 1986.

[37] C. Grand, J. Arrault and M. E. Cates, "Slow Transients and Metastability in Wormlike Micelle Rheology," *J. Phys. II France,* vol. 7, pp. 1071-1086, 1997.

[38] K. Hyun, M. Wilhelm, C. O. Klein, K. S. Cho, J. G. Nam, K. H. Ahn, S. J. Lee, R. H. Ewoldt and G. H. McKinley, "A review of nonlinear oscillatory shear tests: analysis and application of large amplitude oscillatory shear (LAOS)," *Progress in Polymer Science,* vol. 36, pp. 1697-1753, 2011.

[39] S. Shin, K. D. Dorfman and X. Cheng, "Shear-banding and superdiffusivity in entangled polymer solutions," *Physical Review E,* vol. 96, p. 062503, 2017.

[40] C. Chicone, Ordinary Differential Equations with Applications, New York, NY: Springer, 2000.

[41] P. Politi and C. Misbah, "When does coarsening occur in the dynamics of one-dimensional fronts?," *Physical Review Letters,* vol. 92, no. 9, p. 090601, 2004.

[42] J. Cahn and J. E. Hilliard, "Free Energy of a Nonuniform System. I. Interfacial Free Energy," *Journal of Chemical Physics,* vol. 28, p. 258, 2004.

[43] P. W. Bates and P. C. Fife, "The dynamics of nucleation for the Cahn Hilliard equation," *SIAM J. Appl. Math.,* vol. 53, no. 4, p. 990, 1993.